

Pontificia Universidad Católica del
Perú



Investigating the potential of magnetic arc oscillated GMAW-Welding for hard surfacing applications

MASTER THESIS

Student

Falk Nagel (B. Sc.)

Matriculation number

201245257

Due date

Monday 22nd April, 2013

Supervised by

Prof. Dr.-Ing habil. Jean Pierre Bergmann

Dipl. Ing. Karsten Gunther

Dr. Francisco Rumiche

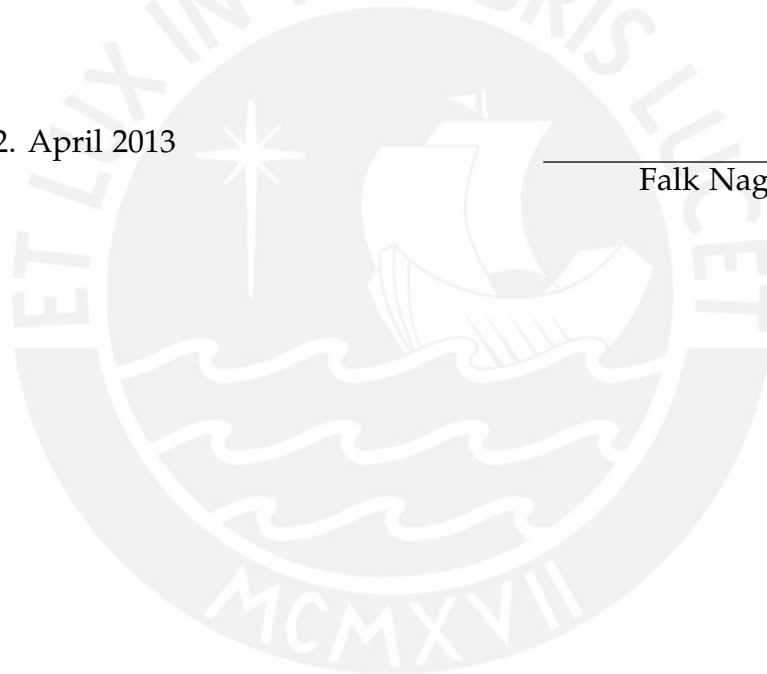
Lima 2012

Selbstständigkeitserklärung

Ich versichern hiermit, dass ich die vorliegende Arbeit selbständig und ohne Benutzung anderer als der angegebenen Hilfsmittel angefertigt haben. Alle Stellen, die wörtlich oder sinngemäß aus veröffentlichten und nicht veröffentlichten Schriften anderer entnommen sind, sind als solche kenntlich gemacht. Die Arbeit ist in gleicher oder ähnlicher Form noch nicht als Prüfungsarbeit eingereicht worden. Ich habe die Hinweise für das Anfertigen wissenschaftlicher Arbeiten zur Kenntnis genommen.

Ilmenau, den 22. April 2013

Falk Nagel (B. Sc.)



Kurzfassung

Das Metallschutzgasschweißen mit Fülldrahtelektrode ist ein in der Industrie verbreitetes Verfahren zur Herstellung von Hartpanzerungen. Charakteristisch ist die gezielte Beeinflussung des Schweißprozesses und der chemischen Zusammensetzung des Schweißguts durch die Auswahl der Füllstoffe. Des Weiteren können dem Fülldraht Stoffe hinzugegeben werden, wodurch das Schweißen ohne Schutzgas durchgeführt werden kann. Nachteilig ist jedoch der hohe Aufmischungsgrad bei diesem Verfahren. Eine Möglichkeit, diesem Effekt entgegenzuwirken, besteht darin, den Lichtbogen durch das Anlegen eines Magnetfelds in eine oszillierende Bewegung zu versetzen.

Der Einfluss eines oszillierenden transversalen Magnetfeldes auf die Nahtausbildung beim MSG-Schweißen mit Fülldraht wurde untersucht. Es zeigt sich dabei, dass der Einbrand verbreitert und die Einbrandtiefe durch die gezielte Auslenkung verringert werden konnte. Der Einfluss des magnetischen Pendelns ist beim Kurzschlusslichtbogen kleiner als beim Impulslichtbogen. Bei hohen Frequenzen und hoher Flussdichte wurde außerdem eine Verringerung der Prozessstabilität und eine daraus resultierende Verschlechterung der Schweißnahtausbildung festgestellt. Außerdem führte ein starker Einfluss des Magnetfelds zu einer erschwerten Tropfenablösung beim Impuls- und Sprühlichtbogen.

Abstarct

The flux cored arc welding process has some characteristic features and is therefore established in the industry to fabricate hardfacing. One advantage of the process is the possibility to vary the alloy content of the weld metal by manipulating the chemical composition of the filler material. Moreover, it is possible to produce self shielding electrodes, which show advantages for outdoor applications. On the other hand this process creates high dilution rates. One possibility to avoid this effect is to apply a magnetic field in order to deflect the welding arc.

In this thesis, the influence of a transversal magnetic field on the weld seam formation during FCAW was investigated. An increase of the weld width and a simultaneous decrease of the penetration depth was achieved at a certain deflection. The influence of the magnetic oscillation was found to be stronger for short circuit mode than for pulsed mode. Furthermore, high frequencies in combination with a high magnetic flux density caused a reduced process stability and consequently a worsening of the weld bead appearance. Apart from that, the drop detachment was inhibited, when a strong magnetic field was applied during pulsed and spray mode.

Contents

1	Motivation	1
2	State of the art	2
2.1	Wear	2
2.2	Hardfacing materials	3
2.3	Deposition welding	4
2.4	Flux cored arc welding	8
2.4.1	Characteristics of the power source	9
2.4.2	Electrodes	9
2.4.3	Arc characteristics	11
2.4.3.1	Acting forces on the arc and metal droplets	13
2.4.3.2	Metal transfer	13
2.4.4	Shielding gas	16
2.5	Influence of oscillation on the weld	18
2.5.1	Generation of oscillation	18
2.5.1.1	Mechanical oscillation	18
2.5.1.2	Magnetic oscillation	20
2.5.2	Effects on the weld	23
2.5.2.1	Weld pool stirring	23
2.5.2.2	Oscillation	24
3	Objective	27
4	Experimental procedure	28
4.1	Materials	28
4.1.1	Base material	28
4.1.2	Weld deposit	28
4.2	Equipment	29
4.2.1	Welding equipment	29
4.2.2	Magnetic circuit	29

4.3	Processing	31
4.4	Engaged readings recorders	33
4.4.1	Video capturing	33
4.4.2	Welding current	34
4.5	Sample characterization	34
4.5.1	Metallography	34
4.5.2	SEM analysis	35
4.5.3	Hardness	35
5	Results and discussion	36
5.1	Magnetic circuit	36
5.2	Welding results	37
5.2.1	Short circuit	37
5.2.1.1	Material transfer characteristics	37
5.2.1.2	Weld seam appearance	40
5.2.1.3	Metallography	43
5.2.1.4	SEM analysis	44
5.2.1.5	Hardness	44
5.2.2	Pulsed transfer mode	47
5.2.2.1	Material transfer characteristics	47
5.2.2.2	Weld seam appearance	51
5.2.2.3	Metallography	53
5.2.2.4	SEM analysis	55
5.2.2.5	Hardness	56
5.2.3	Spray mode	56
5.2.3.1	Material transfer characteristics	56
5.2.3.2	Weld bead appearance	57
5.3	Error consideration	60
6	Summary	61
7	Outlook	62
	List of Tables	LXVIII
	List of Figures	LXXI
	List of abbreviations and formula symbols	LXXII



1 Motivation

According to the German association for tribology [Ges], the costs of friction and wear can amount 5% of the gross domestic product per year for industrial countries. Regarding Germany for example, it values 35 billion Euro per year. By analyzing and optimizing the tribological system, 5 billion Euro can be saved according to this association.

Hardfacing by deposition welding is one possibility to increase the lifetime and reliability of a product. Standard processes are gas metal arc welding (GMAW), plasma transformed arc welding (PTA) and others. In order to coat great areas, these processes have already been established in the industry. Characteristic features of PTA are the high deposition rate and the low dilution. Restrictions have to be made due to the complexity and the production costs. GMAW shows advantages like lower production costs, simplicity and good deposition rates. Due to the use of flux cored electrodes, the chemical composition of the weld can be influenced positively. Nevertheless, the dilution reaches values up to 30%.

When it comes to staying competitive within the section of technical equipment and tools, it is all about time. Innovative hardfacing technologies can insure, that downtime and maintenance cost are kept as low as possible. One approach is the increase of the weld width due to an oscillation of the welding gun. For this application, mass and inertia represent a limit for the potential. Another method is to deflect the arc by an external magnetic field in order to increase the weld width. Investigations have been carried out on PTA, GMAW and gas tungsten arc welding. The effect of the magnetically deflection of the arc for FCAW has not been regarded so far.

2 State of the art

2.1 Wear

Wear can be defined as the continuous loss of material of a solid body, resulting from mechanical burden. It can be superimposed by corrosion. The main actors are surface spallation, adhesion, abrasion and tribochemical reactions [Sch10].

Wear and friction are considered, where surfaces interact in an ambient medium under burden and relative movement [WD11]. This fact is illustrated schematically in figure 2.1.

The point of this reflection is, that wear and friction are no material properties, instead they are caused by the interaction of different materials, lubricants, forces, velocities and environment influences (see [WD11]).

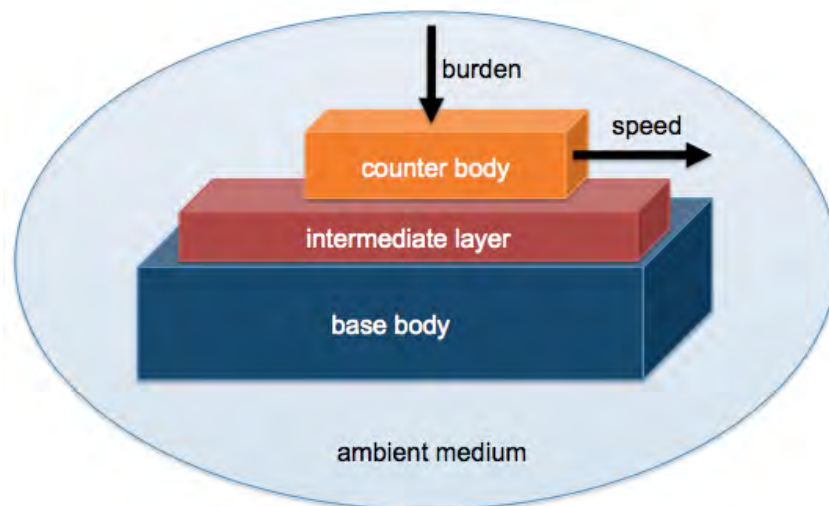


Figure 2.1: Schematic illustration of the tribological system (see [WD11])

Tribological problems can be encountered in several technical applications. The aim of this concept according to Weissbach [WD11] is to:

- reduce friction and increase efficiency,
- minimize wear and increase lifetime and liability,
- decrease consumption of lubricant and thus reduce maintenance costs and
- use regenerated design of wear parts in order to reduce maintenance costs.

2.2 Hardfacing materials

For conventional hardfacing applications, materials like steel, low-alloy ferrous materials, chromium white irons, high-alloy ferrous materials, carbides, nickel- or cobalt-based alloys are used. From the metallurgical point of view, hardfacing alloys consist of hard phase precipitates such as borides, carbides, or intermetallics bound in a softer iron-, nickel-, or cobalt-based alloy [AO93]. Furthermore multi-component systems like tungsten carbide and Fe-Cr-V-C have to be named in context of hardfacing materials. The wear resistance of the deposit strongly depends on the hardness of the hard particles, their volumetric content, as well as their size and distribution within the matrix [Geb98].

Iron-based alloys can be divided into pearlitic-, austenitic-, martensitic steels and high-alloy irons. The last mentioned generally contain a large amount of chromium and/or molybdenum carbides usually within a martensitic matrix. The carbon content ranges from 2% to 6%, providing large amounts of carbides [AO93].

The most important microstructural feature in the high-chromium irons, at least from a wear point of view, is the M_7C_3 carbide, which forms in abundance during solidification and contains chromium, iron, and (if present) molybdenum. The matrix around these carbide particles can be austenitic, pearlitic, or martensitic [AC52]. In general, the austenitic alloys rely on manganese for austenite stability [AO93].

At high carbon and chromium levels the formation of a hypereutectic microstructure, containing large, spinelike carbide particles (with a hexagonal cross section), is favored. At lower carbon and chromium contents, the microstructure is hypoeutectic [AO93].

High chromium alloys are used for strong abrasion and little or no impact applications like earth moving.

2.3 Deposition welding

To protect the workpiece surface against abrasion, impact, erosion, galling and cavitation, coatings are used. In general, coatings can be classified according to DIN 8580, which is illustrated in figure 2.2. In order to realize the design rule "functional material at the point of function" [Kra00], hardening processes like ion implantation, nitriding, flame hardening, welding or spraying are available.

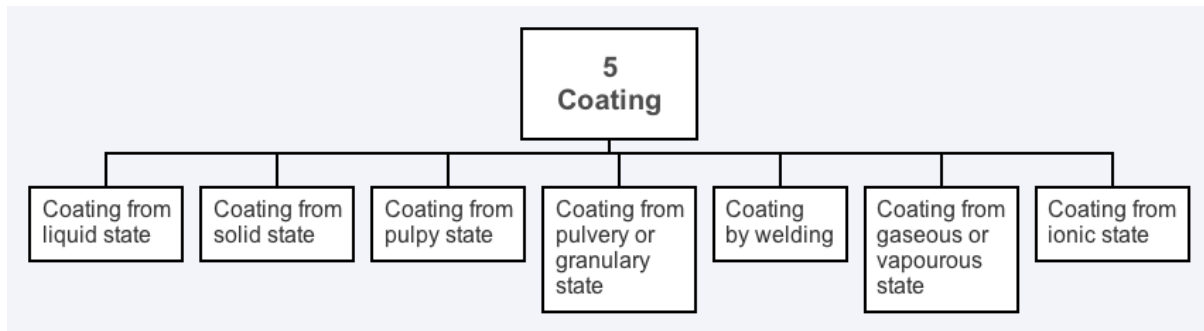


Figure 2.2: Designations of main group 5 of the norm DIN 8580 [DIN03]

Deposition welding is used to maintain workpieces as well as add functionality to a compound. The term hardfacing is used for certain processes, that increase the workpiece wear resistance. When enhancing chemical resistance, the term cladding is used. Adding a layer to combine nonsimilar materials is called buffering. The economical benefits of hardfacing are [AO83]:

- increased productivity by less downtime for repair,
- enhanced efficiency by permitting higher applied loads,
- reduced maintenance costs due to reclamation of worn parts and
- optimum combination of wear and toughness by the use of less expensive and tougher material.

The following major deposition welding processes will be introduced briefly and the key figures are summarized in table A.1:

Electroslag welding

Electroslag welding (ESW) belongs to resistance welding. An arc is ignited between the workpiece surface and the electrode, melts the flux and forms the slag. Then the arc extinguishes because of the conductivity of the molten slag and the electric current

keeps it molten. The generated heat is sufficient to fuse the welding electrode and the surface of the workpiece. The temperature of the bath is approximately 2000 °C and the surface temperature is about 1650 °C [Ame91].

Submerged arc welding

An arc burns between a continuously fed wire and the workpiece. Thus, arc and molten metal are submerged in a granular flux, which protects them from the environment. The flux influences the stability of the arc as well as mechanical and chemical properties of the weld [Ame91].

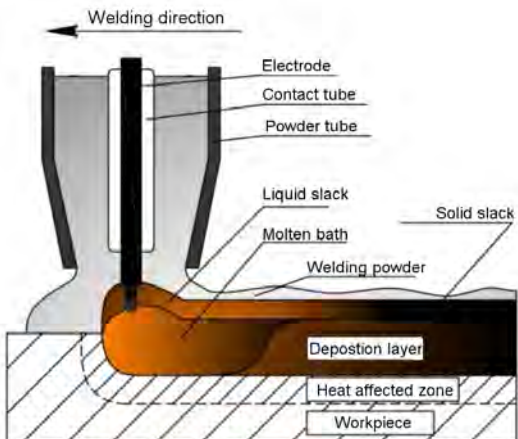
Laser deposition welding

Under specific parameters the laser beam melts filler and base material up to a penetration of 0.3 mm. Mostly, the filler material is added in form of powder, but solid wires are used as well. Diode laser systems are used commonly [FSTW11].

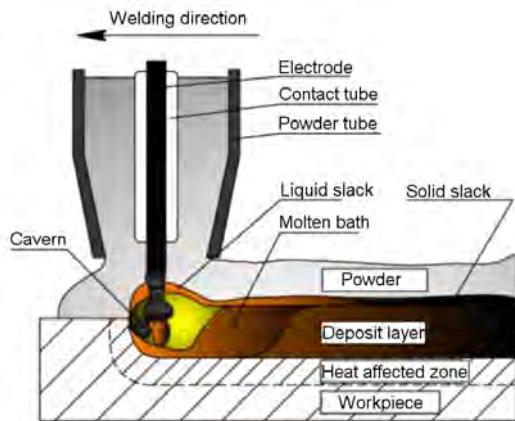
Plasma arc welding

Plasma arc welding (PAW) is an extension of gas tungsten arc welding (GTAW). It is described as "an arc welding process that produces coalescence of metals by heating them with a constricted arc between an electrode and the workpiece (transferred arc) or between the electrode and the constricting nozzle (nontransferred arc)" [Ame91]. Filler materials are added as powder or pre-heated wire.

Table 2.1: Summary of important deposition welding processes [Teu02]

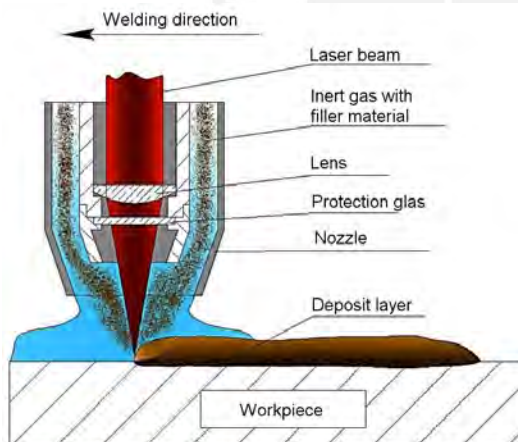
Electroslag welding (ESW)	
	<ul style="list-style-type: none"> • width of the strip electrode up to 180 mm • rate of deposition up to 20 kg/h • area efficiency up to 0.5 m²/h • dilution rate from 8 % to 10 % • higher travel speed compared to SAW

Submerged arc welding (SAW)



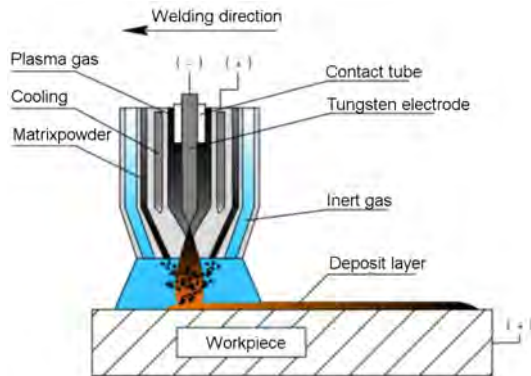
- strip or round electrodes (solid or tubular)
- width of strip electrodes up to 200 mm
- deposition rate from 10 kg/h to 40 kg/h
- area efficiency from 0.3 m²/h to 0.9 m²/h
- dilution rate from 13 % to 40 %
- layer thickness from 5 mm to 8 mm
- only downhand position

Laser welding



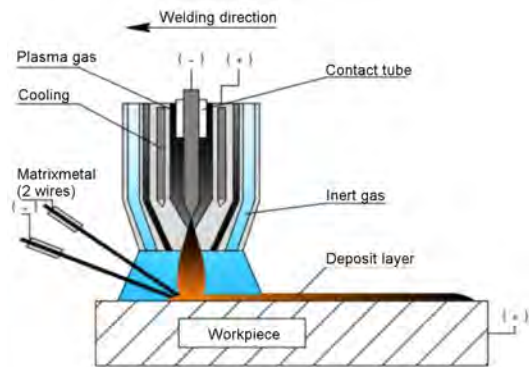
- wire or powder filler material
- deposition rate from 1 kg/h to 2 kg/h
- dilution rate from 13 % to 40 %
- layer thickness from 0.2 mm to 2 mm
- low efficiency
- high energy density

Powder plasma welding



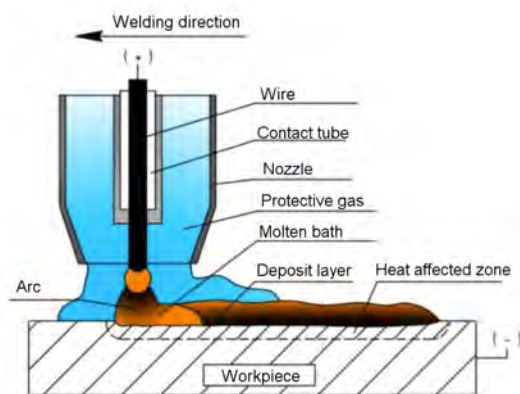
- deposition rate from 6 kg/h to 25 kg/h
- dilution rates from 5 % to 10 %
- layer thickness from 0.5 mm to 6 mm

Hot wire plasma welding



- deposition rate from 10 kg/h to 30 kg/h
- dilution rate from 5 % to 30 %
- layer thickness from 2 mm to 5 mm

Gas metal arc welding (GMAW)



- protective gas (inert or active)
- deposition rate up to 15 kg/h
- area efficiency up to 0.3 m²/h
- dilution rates from 13 % to 30 %
- layer thickness from 2 mm to 8 mm
- high heat input
- irregular weld penetration

2.4 Flux cored arc welding

Flux cored arc welding (FCAW), also known as MIG welding with flux cored electrode, combines characteristics of gas metal arc welding (GMAW), shielded metal arc welding (SMAW) and submerged arc welding (SAW) namely the following:

- the productivity of continuous wire welding,
- the metallurgical benefits that can be derived from a flux and
- a slag that supports and shapes the weld bead.

FCAW is an arc welding process, where the arc burns between the continuous fed filler wire and the workpiece. In general, it can be divided into two types: gas-shielded and self-shielded type. The first one is illustrated in figure 2.3 and the second in figure 2.4. Usually, carbon dioxide or mixtures of argon and carbon dioxide are used to protect the weld from the atmosphere. For the self-shielding method, the protection is realized by the vaporized flux ingredient which produces carbon dioxide [Ame91]. Therefore, the shielded method can be assigned to GMAW and the self-shielding type to open arc welding.

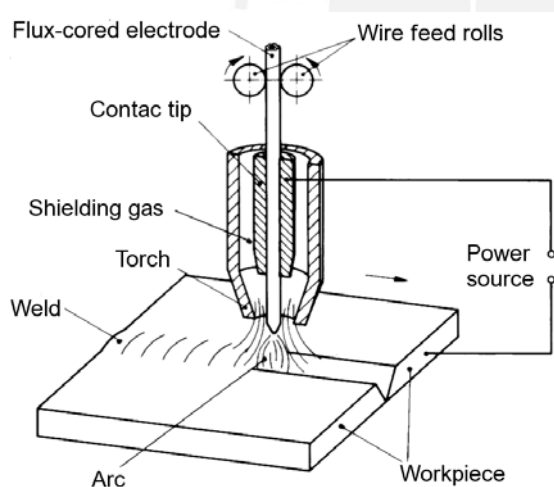


Figure 2.3: Scheme of shielded FCAW [DIN05]

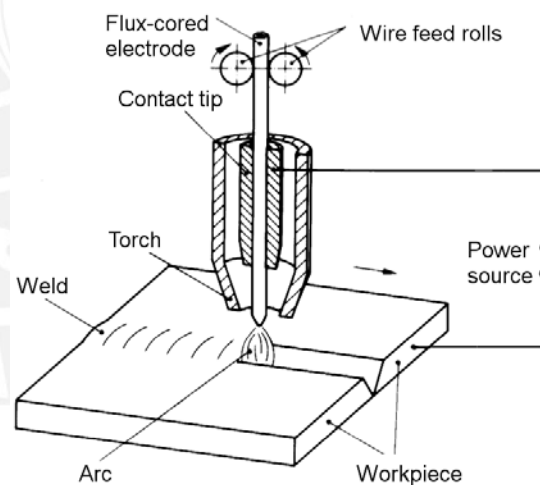


Figure 2.4: Scheme of self-shielded FCAW [DIN05]

According to the Welding Handbook [Ame91], FCAW is characterized by high-quality weld metal deposits and a smooth and uniform weld appearance. Other benefits are the high deposition rate and relatively high deposit efficiency. On the other side, this process can produce slag, which must be removed and the electrodes are more

expensive compared to solid wires on weight basis. The application also produces hazardous smoke and fumes.

2.4.1 Characteristics of the power source

For GMAW and FCAW, constant voltage power supplies are used. As it can be seen in figure 2.5, the characteristic curve is nearly constant or slightly descending. The characteristic curves of different arc lengths are also diagrammed in the figure. A decrease of the arc length results in a large change of the welding current, which causes more heat input into the wire. More material can be molten leading to a decrease of the arc length until the process is stable. There is no inertia, which causes the internal regulation to be very fast.

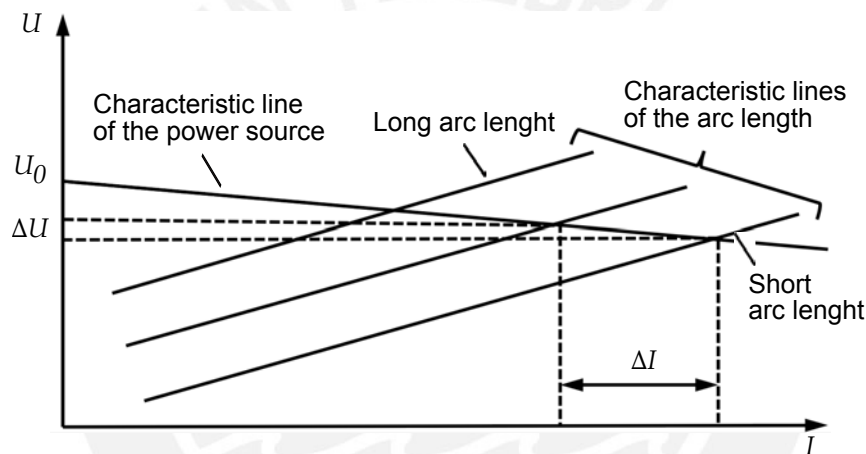


Figure 2.5: Characteristics of arc length and the power supply

2.4.2 Electrodes

The wire is made from alloy steel or low carbon steel filled with dry powder of flux and/or alloying material. The composition can vary depending on the standards and the manufacturer of the electrode. Examples are given in table 2.2. Because of the selection of the ingredients for core and sheath, the following possibilities can be realized (see [Ame91]):

- produce welding characteristics ranging from high deposition rates in the flat position to proper fusion and bead shape in the overhead position.
- produce electrodes for various gas shielding mixtures and for self shielding.

- vary alloy content of the weld metal from mild steel for certain electrodes to high alloy stainless steel for others.

Table 2.2: Standards for Tubular cored electrodes

Standard	Designation
DIN EN ISO 12153	Electrodes for gas shielded and non-gas shielded metal arc welding of nickel and nickel alloys
DIN EN ISO 17632	Electrodes for gas shielded and non-gas shielded metal arc welding of non-alloy and fine grain steels
DIN EN ISO 17633	Electrodes and rods for gas shielded and non-gas shielded metal arc welding of stainless and heat-resisting steels
DIN EN ISO 17634	Electrodes for gas shielded metal arc welding of creep-resisting steels
DIN EN ISO 18276	Tubular cored electrodes for gas-shielded and non-gas-shielded metal arc welding of high strength steels

Electrodes for FCAW can be divided into three categories: basic, rutile and metal cored wires. Basic and rutile wires induce slag, whereas metal cored wires do not result in slag. Therefore, the mechanical and chemical properties of the weld seam are mainly influenced by the type of powder of the flux core wire (see [FSTW11]).

According to [Ame91], the functions of the components are:

- act as deoxidizers or scavengers to help purify the metal and produce a sound deposit,
- form slag to float on the molten weld metal and protect it from the atmosphere during solidification,
- act as arc stabilizers to produce a smooth welding arc and reduce weld spatter,
- add alloying elements to the weld metal to increase weld strength and to provide other required weld-metal properties,
- provide shielding gas.

Basic electrodes produce a very fluid slag with a relatively low solidification temperature. As it is difficult to operate in spray mode, short circuiting mode is the alternative in order to realize out of position welding. The weld shows high purity, leading to good mechanical properties. The best welding results are achieved with negative polarity of the electrode [WL06].

Good weldability and possibility to weld out of position with a high productivity are some of the key features of rutile electrodes. The wire produces a more fluid slag, that solidifies at a lower temperature. Therefore, the weld bead becomes flat and the surface is bright and smooth.

Metal cored wires do not form slag like rutile and basic ones. The deposit efficiency ranges between 95 % and 96 % and for rutile and basic wires between 82 % and 88 %.

A list of common used elements, their sources and their purpose is presented in table 2.3. Deoxidizers like silicon and manganese are added to counteract the burn of alloying elements (Cr, Al, V, Mn, Si) due to oxidation. Aluminum reacts with nitrogen to form stable nitrides and prevents the formation of porosity [Ame91].

Because of the smaller conducting cross sectional area, tubular wires show a higher resistance than solid wires. This also leads to an increased preheating of the electrode extension and deposition rate. Smoke emission and spatter are disadvantages of this process [Dil06].

2.4.3 Arc characteristics

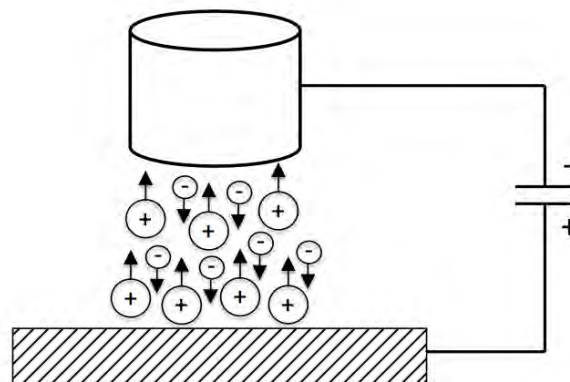


Figure 2.6: Flux of the current within the arc

Basically, an electric arc is a discharge between two electrodes in gas through ionization of the gas molecules. In general, the gas has a very low electrical conductivity [FSTW11].

Caused by the application of an electrical field between the electrodes, the electrical charged particles are accelerated to the opposite poles. It is important to point out, that the electrons have no mass and are charged negative. Therefore, they can be accelerated

Table 2.3: Common core elements in flux cored electrodes [Ame91]

Element	Standard	Designation
Aluminum	Metal powder	Deoxidize and denitrify
Calcium	Minerals such as fluorspar (CaF ₂) and limestone (CaCO ₃)	Provide shielding and form slag
Carbon	Element in ferroalloys such as ferromanganese	Increase hardness and strength
Chromium	Ferroalloy or metal powder	Alloy to improve creep resistance, hardness, strength and corrosion
Iron	Ferroalloys and iron powder	Alloy matrix in iron base deposits, alloy in nickel base and other nonferrous deposits
Manganese	Ferroalloy such as ferromanganese or as metal powder	Deoxidize; prevent hot shortness by combining with sulfur to form MnS; increase hardness and strength; form slag
Molybdenum	Ferroalloy	Alloying to increase hardness strength, and in austenitic stainless steels to increase resistance to pitting-type corrosion
Nickel	Metal Powder	Alloying to improve hardness, strength, toughness and corrosion resistance
Silicon	Ferroalloy such as ferrosilicon or silicomanganese; mineral silicates such as feldspar	Deoxidize and form slag
Sodium	Minerals such as sodium-bearing feldspars and silicates in frits	Stabilize the arc and form slag
Titanium	Ferroalloy such as ferrotitanium; in mineral, rutile	Deoxidize and denitrify; form slag; stabilize carbon in some stainless steels
Zirconium	Oxide or metal powder	Deoxidize and denitrify, form slag

easily and transform energy. During the collision with other molecules, they can knock out other electrons and thus form ions and electrons. The electrons move to the anode and the positive charged ions move to the cathode. This fact is illustrated in figure 2.6. In this case the electrical conductor is plasma [FSTW11].

To maintain the arc, field electron emission and thermionic emission are important. The field emission is the emission of electrons induced by an electrostatic field and their amount depends on the voltage of the electrostatic field. The thermionic emission results when heat is applied to a metal workpiece and electrons are emitted on the surface.

2.4.3.1 Acting forces on the arc and metal droplets

Every current-carrying conductor is surrounded by a circular magnetic field. This field produces a radial force, which is orientated towards the center, namely the Lorentz force. This force tries to pinch the electrical conductor [Dil06]. The other forces are the gravity and the drag force from the plasma jet. Moreover the surface tension and the repelled force of the evaporating material have to be considered as well.

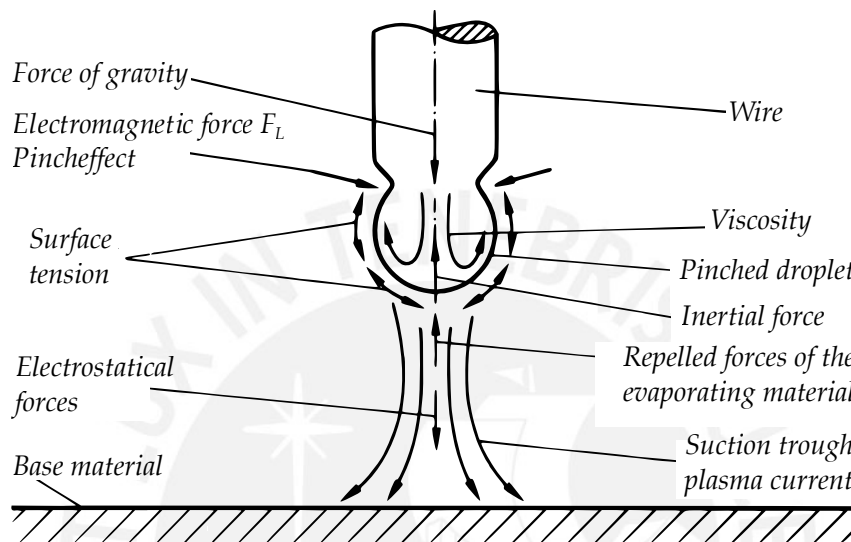


Figure 2.7: Forces acting on the droplet [Dil06]

2.4.3.2 Metal transfer

Below, a classification of the transfer modes is presented according to Iordachescu et al. [IQ08], which is similar to that of the International Insitute of Welding classification. An overview is given in figure 2.8. Short circuiting, spray and pulsed transfer mode are used mainly for GMAW while short circuiting and globular mode are used for FCAW. Spray transfer mode can also be applied, but is only considered as an "almost true spray mode" and strongly depends on the current and composition of the flux [BOC07].

Short circuiting arc

One typic feature of short circuit arc welding is the low heat input into the weld. The tip of the wire starts to melt, but no droplet is released. Continuous feeding rate of the wire and growing droplet finally lead to contact of the wire and the base material

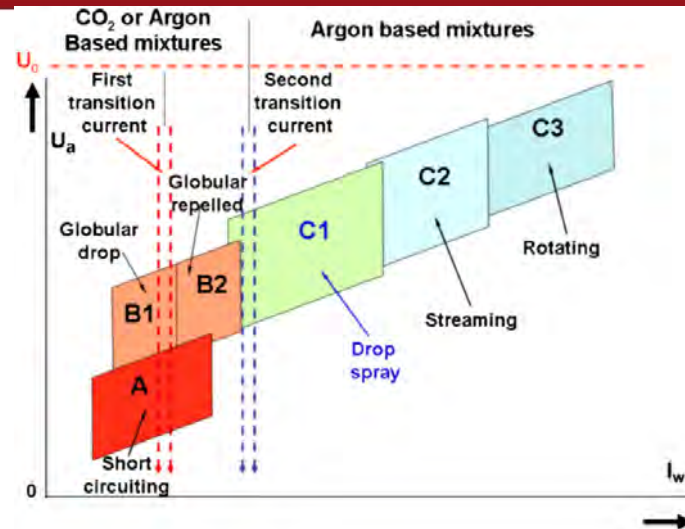


Figure 2.8: Transfer modes in an $I - U$ - Diagram [IQ08]

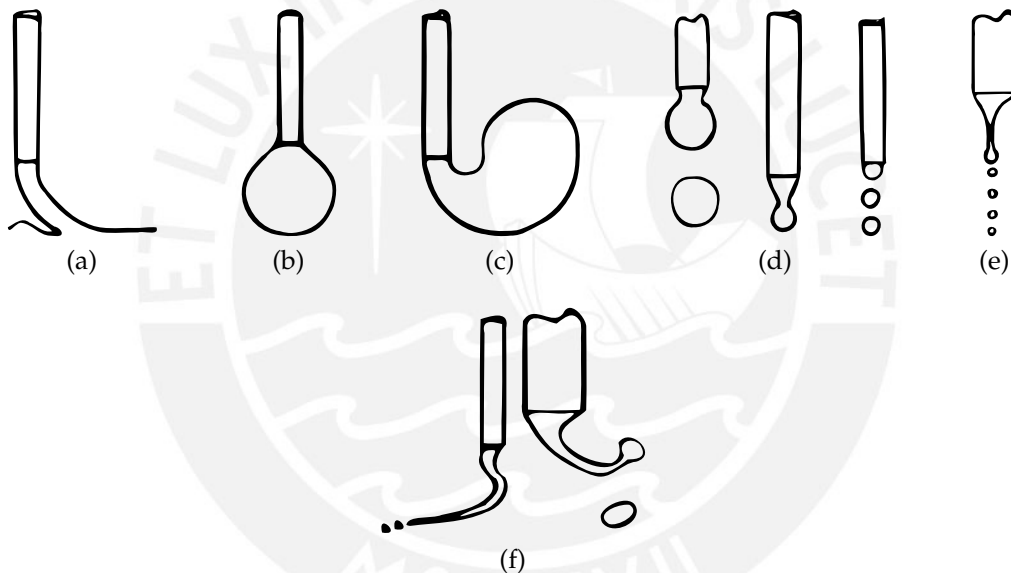


Figure 2.9: Arc transfer modes according to [IQ08]: (a) Short Circuit, (b) Globular Drop, (c) Globular Repelled, (d) Drop Spray, (e) Streaming, (f) Rotating

resulting in a short circuit as shown in figure 2.9a. The tail of the droplet will be constricted by the Lorentz force. It forms a gap of ionized metal vapor and a new arc can ignite [Dil06, WL06].

Globular arc

By using the same welding current as for short circuiting arc but a higher voltage, the amount of short-circuits is decreased and leads to a short circuit free transfer mode.

Bigger droplets than the diameter of the electrode of molten metal are distinctive for this mode (see figure 2.9b). According to Iordachescu et al. [IQ08], an increase of the welding current results in globular repelled transfer mode, which is characteristic for the use of CO₂ in GMAW. The molten drop is rejected upwards (see figure 2.9c) resulting in spatter. For both transfer modes, gravity force is the principal factor for drop detachment.

Drop spray

Above a certain welding current and high voltages, the transfer mode can be characterized as short-circuit-free and fine droplet detachment (see figure 2.9d). The heat input and the deposition rate are high. The magnetic force contributes the wire and therefore supports the drop release. Pure Argon or a gas mixture of argon and maximum 25 % of CO₂ or a few percent of O₂, has to be used.

Streaming and rotating

The drops become smaller and more frequent like a shower, which is shown in figure 2.9e, at increased current. At high values, the stream starts to rotate (see figure 2.9f). According to Dilthey [Dil06], this phenomenon requires welding currents above 400 A and wire feeding rates between 20 m/min and 40 m/min. The deposition rate can be enhanced in comparison to conventional GMAW. When using high welding currents and long, free wire ends, resistance heating of the wire occurs and results in softening of the wire. Because of the high arc pressure the droplet detachment takes place in form of a rotating movement. The weld bead is extended and flat. Because of the high heat input, this transfer mode is used for heavy machine industry.

Pulsed arc

The power source switches periodically between two levels: a lower base current and a higher impulse current. The background current keeps the ionization constant. Moreover, the arc preheats the tip of the wire and the base material. The detachment of the droplet always occurs during the high current phase. Depending on the parameters, one or more drops can be released. The process is shown in figure 2.10. Dilthey [Dil06] mentions a minimum share of 80 % of argon for the gas mixture. The frequency of the droplet detachment depends on the power supply and its characteristics.

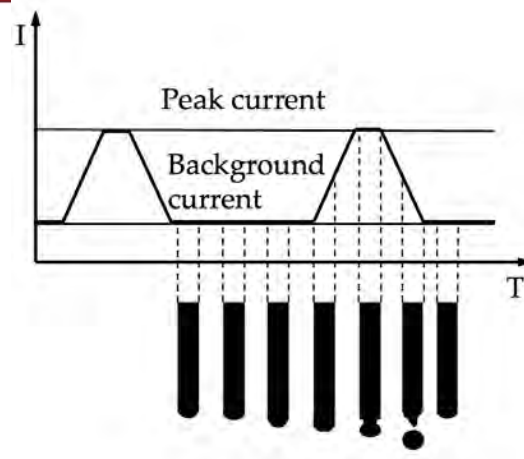


Figure 2.10: Pulsed GMAW current according to Wemann [WL06]

2.4.4 Shielding gas

Shielding gases are divided as:

- inert
 - argon,
 - helium,
- active
 - carbon dioxide,
 - oxygen,
 - and nitrogen.

Their function is to protect the weld bead, the electrode and the arc from atmospheric gases. Moreover, it influences the property of ignition, stability and form of the arc. Gases with low ionization potential facilitate the ignition of the electric arc and those with low thermal conductivity tend to increase the arc stability. Furthermore, it affects the chemical composition and the penetration of the bead and can improve the welding performance (see [FSTW11]). Shielding gases are standardized by DIN EN 439.

Inert gases are used for welding of non-ferrous metals like aluminum, magnesium, titanium and copper. As well, the gases are used for consumable electrodes to avoid the burn of expensive alloying elements. Because of the full outer shell, these noble gases have very low tendency to participate in chemical reactions. Argon has a higher density in comparison to helium and has therefore a better protective effect. Besides argon is cheaper and has a better ignitability. On the other hand, helium results in a hotter arc, higher travel speed and deeper penetration (see [FSTW11, Di106]).

Because of its low thermal conductivity, argon induces a narrow, deep penetrated weld seam. Another characteristic feature is the finger form. Helium shows a higher thermal

conductivity, which produces a radial uniform heat distribution. The weld seam is wider and shows less penetration. Carbon dioxide produces a deep weld bead contour. The influence of the shielding gas of the weld bead contour is presented in figure 2.11.

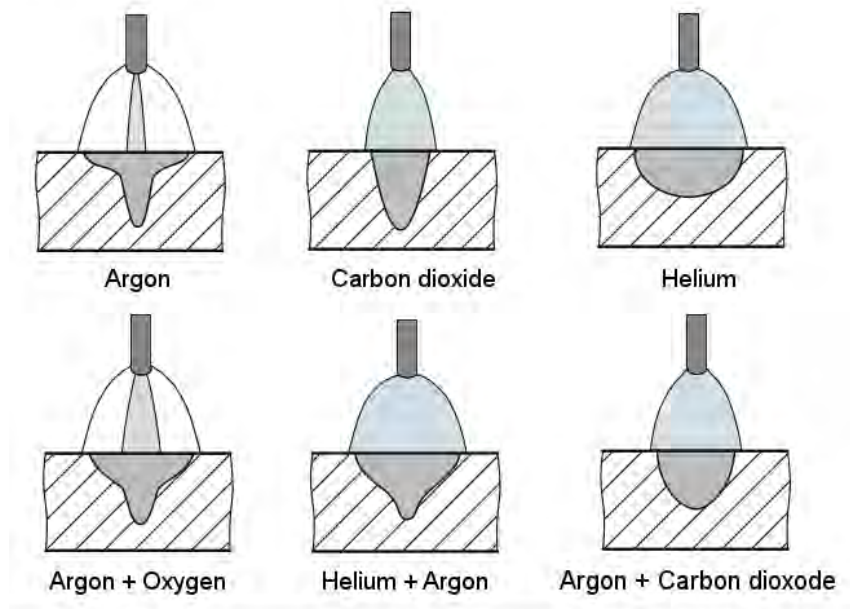


Figure 2.11: Schematic illustration of the influence of shielding gases of the weld bead formation [Sch10]

Carbon dioxide is a common shielding gas and for FCAW the is most widely used. Under room temperature it is inactive but under high temperature CO_2 dissociates to carbon monoxide and oxygen which can be seen in equation 2.1.



The oxygen reacts with the molten metal and hence deoxidizing materials are added to the core of the electrode. Furthermore the molten iron reacts with CO_2 producing iron oxide and carbon monoxide (see equation 2.2).



At red heat temperatures carbon dioxide dissociates to carbon and oxygen, which can be seen in the following equation.



Depending on the carbon concentration of the base material, this gas can lead to a carburization or decarburization. The AWS Handbook [Ame91] names carbon content below 0.05 % of the weld metal when carburization takes place. Above a concentration of 0.1 % the molten weld pool may lose carbon. This is due to the formation of carbon monoxide, because of the oxidizing character of carbon dioxide at high temperatures. Carbon monoxide can cause porosity and therefore deoxidizing materials are added to the core. Oxygen will react with those elements rather than with carbon in steel resulting in solid oxide compounds, which form slag (see [Ame91]). Furthermore, carbon dioxide and oxygen react with the metal and result in metal oxide. These oxides have a lower ionization energy compared to metals and because of that, the electrical conductivity of the arc is better. With high ionization potential, higher voltage is needed, which causes a higher heat input. Because of that, the viscosity is lower and a better degassing can take place. Moreover the surface tension is reduced (see [FSTW11])

According to the Welding Handbook [Ame91], the widely used gas shielding composition consists of 75 % argon and 25 % carbon dioxide. The mixture allows higher tensile and yield strength in comparison to 100 % carbon dioxide shielding gas. Spray transfer mode, out of position welding, greater operator appeal and better arc characteristics can be realized. But the operator has to follow the recommendations of the manufacturer, if the electrodes can be work with such a gas mixture.

2.5 Influence of oscillation on the weld

2.5.1 Generation of oscillation

2.5.1.1 Mechanical oscillation

Several mechanical oscillation systems are available on the market. Common systems can be ordered as optional with welding cars. These systems realize a pendular or linear movement due to an electric motor and a mechanism. Amplitudes, frequency and curve form can be adjusted. The system from Oerlikon [SAF11] can work up to 100 strokes per minute ($f = 1.66$ Hz). The linear system from Merkle [Mer11] offers a travel speed up to 40 mm/s and a travel of ± 25 mm. Industrial robots can be programmed to run these movements as well. The limitation of this systems are the weight, inertia of the mass and the instability of robots above the frequency of 10 Hz [HW85].

A frequency up to 40 Hz was achieved by Kodama [KGKI01] using a magnetic mechanical system. The torch is ratably mounted at the end and a magnetic actuator is installed at the half way. An illustration of the torch can be seen in figure 2.12 and the results of the investigation can be observed in figure 2.13. By using this mechanical

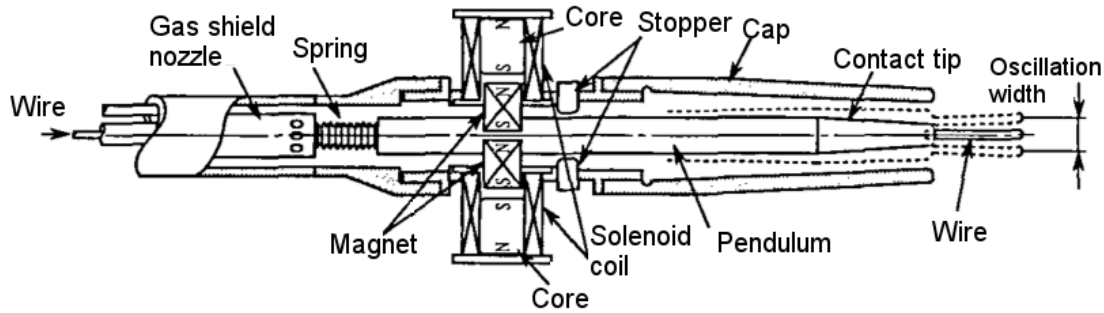


Figure 2.12: Schematic illustration of oscillating torch

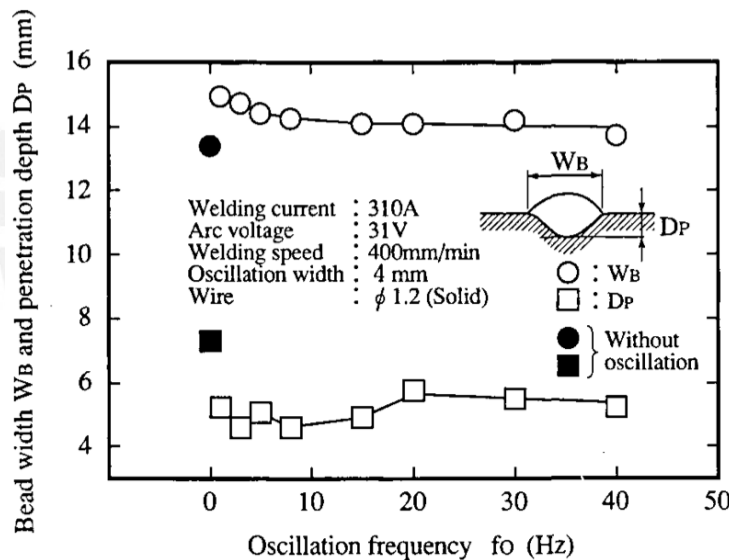


Figure 2.13: Relationship between oscillation frequency and penetration depth and bead width in bead-on-plate welding [KGKI01]

oscillation system with low frequency, the penetration is decreased (30%) and the weld bead width is increased by 11%. The width decreases with increasing frequency until 20 Hz. Between 20 Hz and 40 Hz the width stays constant. In this frequency range, the penetration slightly decreases and under 20 Hz no tendency is observed. For horizontal fillet welding this method shows the tendency of slightly flattened beads.

2.5.1.2 Magnetic oscillation

The arc can be deflected away from the normal arc path by an external magnetic field through the Lorentz force. The Force F acts on a particle, which can be electrons or ions, through an external magnetic field B . This particle has an electric charge q and instantaneous velocity v . The Lorentz force can be calculated according to the following equation:

$$\vec{F} = q \cdot (\vec{v} \times \vec{B}) \quad (2.4)$$

The deflection can be made sideways, backwards or forward depending on the direction of the magnetic field. A transverse magnetic field (TMF) deflects the arc in the welding direction, which is also called longitudinal magnetic oscillation (LMO). Whereas a longitudinal magnetic field (LMF) deflects the arc orthogonal to weld seam. Therefore it is called transversal magnetic oscillation (TMO). These mostly used applications are illustrated in figure 2.14 and figure 2.15. Figure 2.16 shows the installation in order to realize an axial magnetic field.

Two companies offer several systems on the world market ranging from simple one pole, two pole and four pole water cooled system realizing 60 mT. They can be mounted to GMAW and GTAW torches. By using 4 pole systems, circular movements can be made and the diameter of the plasma can be manipulated [JS00].

The magnetic blow effect can be counteracted by a constant transverse magnetic field [Dil76].

Researchers investigated the influence of the oscillated magnetic field of the weld bead for GMAW [KN03, Raz95, Dil76], GTAW [Raz95, KN02], SAW [Raz95, Dil76] and PAW [HW85].

Parameters

The investigations of Dilthey [Dil76] describe, that during the constriction and the droplet detachment, the drops change the release direction, because of the applied external magnetic field. The droplet detaches in the direction of the deflected arc and the forces accelerate the droplet so high, that a change of the direction of the arc will have no effect. This is due the high kinetic energy. The deviation of the arc increases digressively up to 40° with increasing magnetic flux density and under constant current and voltage. Then the deflection increases progressively until the arc extinguishes.

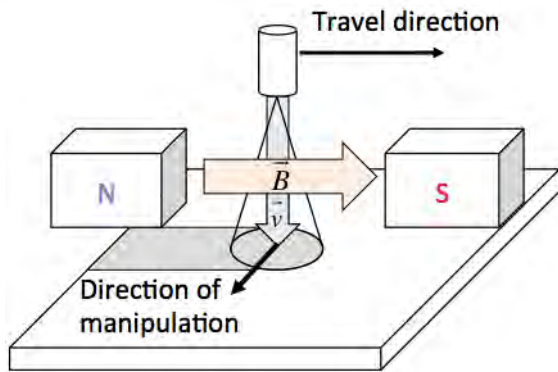


Figure 2.14: Longitudinal magnetic field

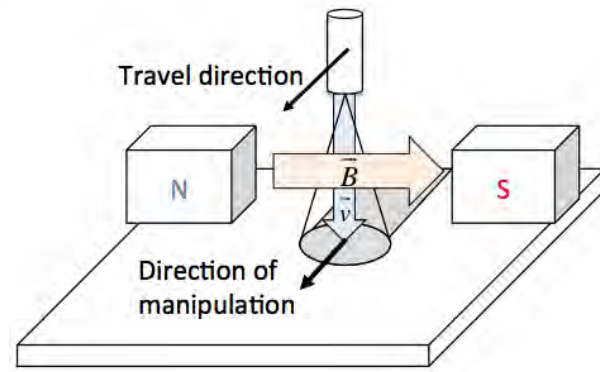


Figure 2.15: Transversal magnetic field

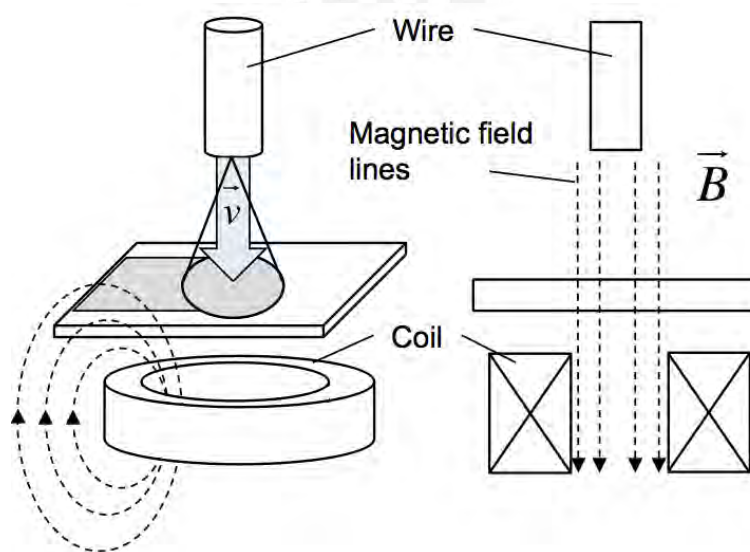


Figure 2.16: Axial magnetic field

For GMAW application, alternating longitudinal magnetic fields are used to increase the width and to decrease the depth of the penetration of weld bead. Alkolov [AK72, Raz95] welded 12Kh18N10T stainless steel with S-08G2S wire, which had a diameter of 1 mm. The weld bead increased from 14 mm to 17 mm using a magnetic flux density of 7.5 mT. The penetration decreased from 2.8 mm to 1.5 mm. Kayboyashi [KN90] achieved an enhancement of the width of 15% and a reduction of the depth of the penetration from 3 mm to 2 mm by using 6 mT and 5 Hz for bead-on-plate GMAW. Filler wire was installed additionally to consumable electrode wire. By increasing the feeding rate of the filler wire, the penetration was reduced. For V-groove welding, the penetration of the groove faces is higher with increasing magnetic flux density, but the root penetration decreases.

Blunt [Blu00] reduced the dilution from 40 % to 13 % and increased the width of the bead from 12 mm to 17 mm using a wire of 1.6 mm and a welding energy range from 1 kJ/mm to 1.4 kJ/mm (short circuit mode). A magnetic field of 6.5 mT and 0.7 Hz was used. A reduction of the dilution from 36 % to 20 % was measured in spray transfer mode (1.8 kJ/mm) using 4 mT and 0.7 Hz. He measured an increased weld bead width of 4 mm/T for short circuiting mode and 1.1 mm/T for spray transfer mode. An example of his results is given in figure 2.17

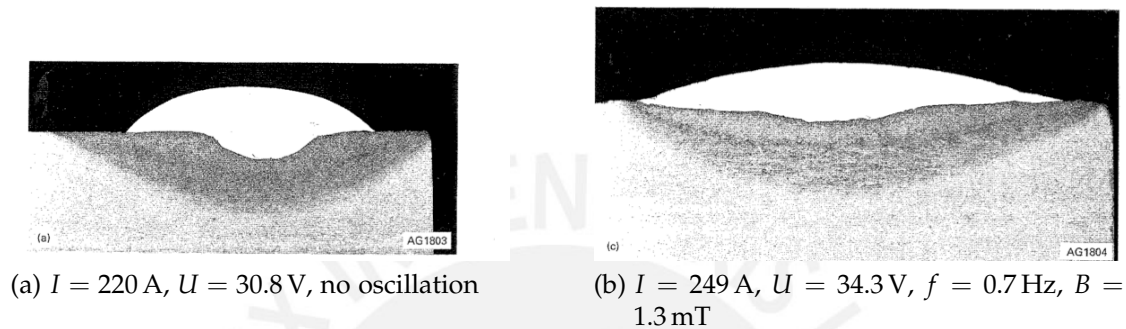


Figure 2.17: The influence of the magnetic oscillation on the weld, spray mode

Kang [KN03] shows the benefits of longitudinal magnetic field for narrow groove welding. Good penetration of the groove faces and root were achieved with 5 mT. Undercut occurred at both groove faces using 7.5 mT. The gap distance is specified with 10 mm.

For SAW, Sheinkin [She69, Raz95] achieved a weld width enhancement between 20 % to 25 %. Furthermore, the electrode melting rate was increased by 10 % to 15 % using magnetic flux density of 8 mT and a frequency of 50 Hz.

The deflection of the arc decreases with increasing welding current under constant voltage and magnetic flux density, because the arc gets stiffer [KN02]. An enhancement of the arc length by increasing the voltage leads to wider range of deflection [Dil76].

Alkolov [AK72, Raz95] mentions extensive spatter by using TMF and spray transfer mode. Kuznetsov [KMSC72] mentions the change from fine droplet transfer to large droplet transfer mode using argon for GMAW applying a longitudinal magnetic field higher than 1.5 mT. The volume of the drop and its existence time to break away increase by a factor from 2 to 3. Satisfactory arc stability are given up to 6 mT. Blunt [Blu00] mentions spatter due to excessive deflection of the droplets above 6 mT for short circuiting mode. Magnetic field strength above 4 mT led to nozzle damage and arc instability in spray mode, but spatter was not a problem.

Yongbing et al. [YZG⁺02] show in their numerical study for GTAW using longitudinal magnetic field the rotation of the molten weld pool. The motion is not axisymmetrical, because of the arc motion. It is also found, that maximal velocity appears at certain annular region deviating weld pool centre. The reason is, that the maximal electromagnetic force applied on weld pool also appears at the annular region.

The numerical study of Yin et al. [YGZS12] shows that the weld becomes more shallow and wider for GTAW with applied axial magnetic field. Because of the circumferential shear stress and the magnetic field, the molten weld pool rotates. The direction of the fluid rotation at the centre of the weld pool is opposite to of the outer regions, because the reverse current flow creates an opposite electromagnetic force. Experimental results from Watanabe et al. [WNE89] shows for austenitic steel GTAW radial stirring of the weld pool. The change of the magnetic field density from 0 mT to 50 mT had a slight influence on the penetration, but a considerably influence on the weld bead. The position of the torch along the travel axis in relation to the magnet was changed. The results show a maximum penetration and a minimum width when the electrode was 2 cm behind the magnet. The position of the electrode changes the appearance of the weld pool from circular to elliptical by increasing the distance. Depending on the sign of the distance, the rotation forms clock- or counterclockwise.

For pulsed GMAW, Dilthey [Dil76] mentions, that by using sufficient magnetic flux density, the arc deflects strongly during the low current phase and can extinguish. Synchronization can solve this problem by applying a magnetic field just during the high current phase. For each phase a specific deflection direction can be assigned.

A further positive effect is the reduction of porosities, because of the "stirring" of the weld pool. By welding plates with different thicknesses, the thickest plate is not fused sufficiently. The use of an offset led to sufficient heat for fusing both plates [Dil76].

2.5.2 Effects on the weld

2.5.2.1 Weld pool stirring

Weld pool stirring can be achieved by using an axial magnetic field, which was mentioned before. Pearce et al. [PK81] achieved an increment of the grain refinement degree in aluminum alloys containing small amount of titanium. They suggested, that the increased grain refinement was due to heterogeneous nucleation, rather than to

dendrite fragmentation. The second mentioned mechanism is the detachment of grains from partially molten regions of the HAZ.

Watanabe et al. [WNE89] concluded from his results, that dendrite fragmentation occurred, because of the reverse motion of the molten metal, which remelted dendrite arms.

2.5.2.2 Oscillation

Kou and Le [KL85] changed the microstructure of 2014 aluminum alloy for GTAW and arc oscillation. Due to the transverse oscillation at low frequencies, dendrite arm spacing was reduced significantly, which can be seen in figure 2.18. It was also observed, that the microstructure appeared more uniform with oscillation than without.

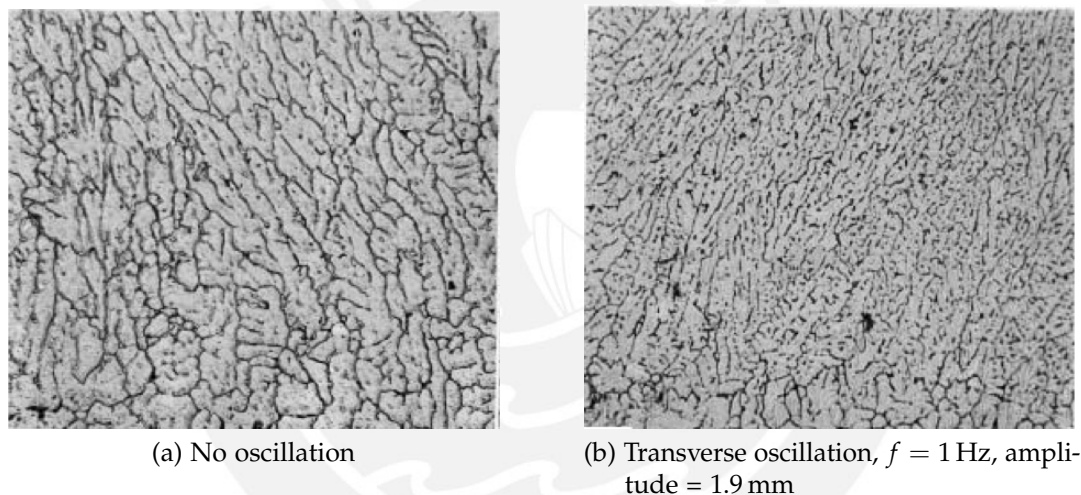


Figure 2.18: Microstructure near fusion line of 2014 aluminum, 200x [Kou03]

The resulting velocity of the molten weld pool with and without oscillation is presented in figure 2.19. By using an oscillation system the velocity u is added by the component v . v is the result of amplitude and frequency. The resulting velocity w is greater than u . Because of the small distance between the heat source and the pool boundary, the temperature gradient is increased, which is valid for small amplitudes. With constant growth rate, the cooling rate increases resulting in a finer microstructure.

Davies and Garland [DG75] achieved a grain refinement in GTAW of Al-2.5 wt % Mg alloy by torch vibration. Resistance to weld solidification cracking was improved in

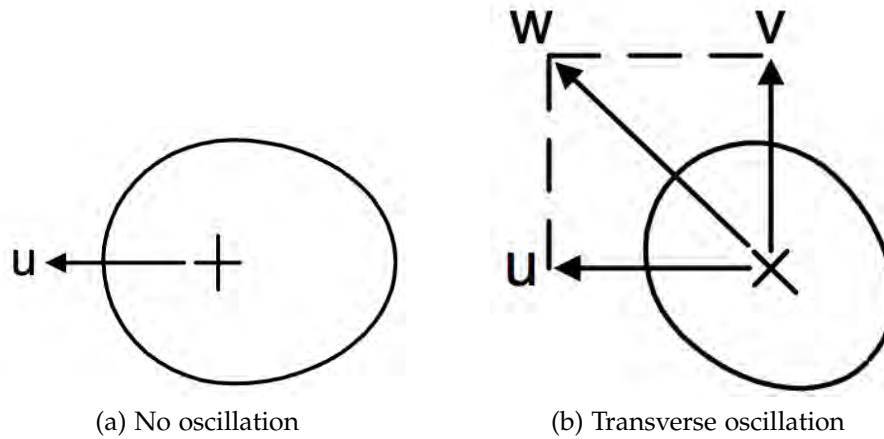


Figure 2.19: Resulting travel speed according to [KL85]

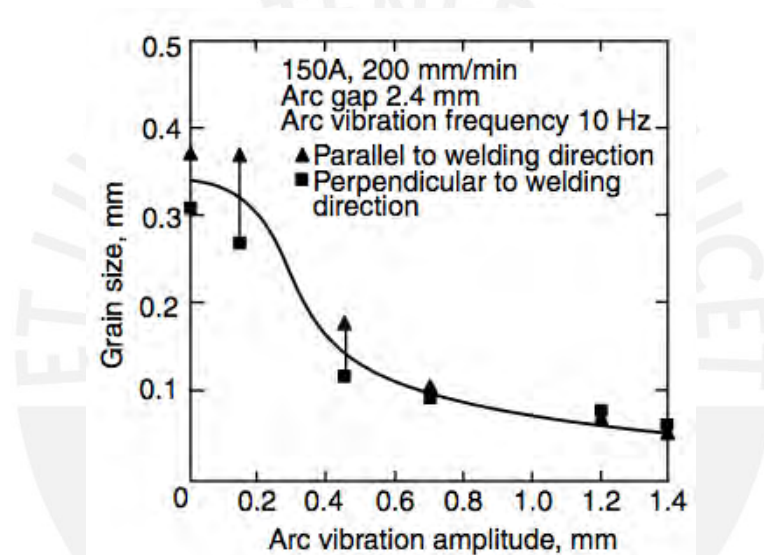


Figure 2.20: Influence of the amplitude of the grain size by torch vibration [Kou03, DG75]

these welds. The effect of the amplitude of torch oscillation on grain size can be seen in figure 2.20. Dendrite fragmentation was proposed as the grain refining mechanism.

Tewari [Tew99] achieved a considerable grain refinement using transversal and longitudinal oscillation for SMAW. The base plate was mounted on a vibrating table. The grain size was reduced from $38 \mu\text{m}$ to $6.2 \mu\text{m}$ under longitudinal oscillation condition of 400 Hz and an amplitude of $5 \mu\text{m}$. $6.7 \mu\text{m}$ were measured under transverse oscillation. The investigator names dendrite fragmentation and grain detachment mechanism as the main actors.

Grain size reduction in the weld bead of around 60% was achieved by Ram et al. [RMS99] for GTAW using alternating LMF for 2090 and 7020 aluminum alloys. The results from the tensile test show an enhancement for the ultimate tensile strength (from 221 MPa to 227 MPa 2090-T3 alloy, from 257 MPa to 275 MPa 7020-T6 alloy). The elongation increased from 8.9% to 12.6% for 2090-T3 and 6.7% to 10.4% for 7020-T6. The effect of grain refinement was only achieved for low frequencies, whereas a frequency of 2.5 Hz led to the best results. An amplitude of 0.6 mm was the most effective. Higher amplitudes led to undesirable arc behavior and lower amplitudes had no effect. The reason for grain refinement were assumed due to the change of weld pool shape and varying direction of maximum thermal gradient. Moreover, an enlarging of the chill zone adjacent to the fusion boundary and the generation of fine-grain bands was observed.

Grain refinement was also identified by using mechanical transverse arc oscillation for GTAW of mid steel (ASTM A36). The amplitude was set to 1.5 mm and frequency to 0.7 Hz. Tensile test showed better results for using oscillation. Grains were finer and relatively equiaxed compared to grains of examples without using TMO. Those were long columnar [MBRM12].

3 Objective

FCAW shows many advantages compared to other welding techniques like lower costs for the welding equipment, good productivity and metallurgical benefits. Due to the fact, that the chemical composition of the deposit can be influenced by the filler material, FCAW fulfills the requirements to realize hardfacing. The disadvantage of the process is the high dilution rate, which ranges from 15 % to 30 % for standard applications. It can be compensated by applying several layers of deposits.

Several investigations have shown, that the weld seam dimensions can be manipulated by magnetic arc oscillation. The penetration depth can be reduced as well as the seam can be widened, which results in economical effects. Nevertheless, investigations on the influence of a transversal magnetic field on the FCAW process have apparently not been carried out so far. Because of the similarity of this process to GMAW, the results should be similar.

The objective of this thesis is to investigate the impact of the arc deflection - realized by an longitudinal magnetic field - on the FCAW process. Therefore several working packages have to be elaborated:

- Realization and characterization of the magnetic circuit,
- Determination of the arc behavior due to the oscillation,
- Analyzation of the influence of the applied magnetic field on the weld seam appearance,
- Definition of the process boundaries.

4 Experimental procedure

4.1 Materials

4.1.1 Base material

ASTM A 36 steel was used for the experiments and the chemical composition is listed in table 4.1. The samples dimensions of 150 x 75 x 12.5 mm and were cut out of steel plate with oxy-fuel gas. The surface was machined using an angle grinder in order to remove impurities and burr.

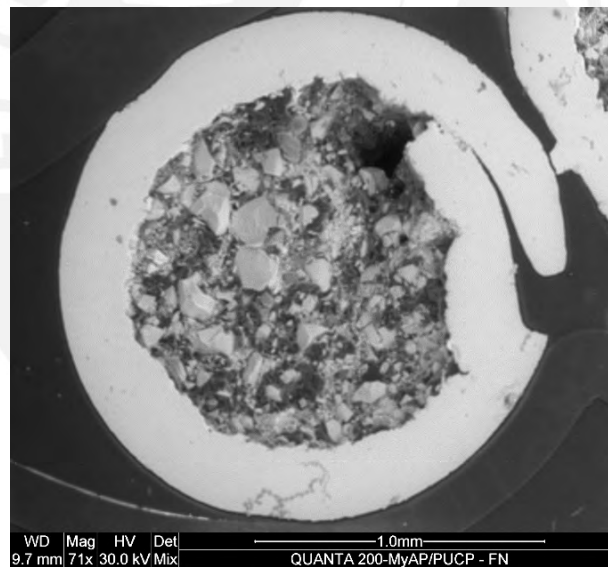


Figure 4.1: Cross section of the wire - SEM analysis

4.1.2 Weld deposit

The flux cored wire (DIN 8555: MF 10-GF-65-GR) with a diameter of 1.6 mm is presented in figure 4.1. The share of the core within the cross section amounts 47.6%. Typical chemical composition of a deposited layer is presented in table 4.1. No shielding gas is

needed according to recommendations of the manufacturer and the stick-out should be set between 15 mm and 25 mm. The hardness of the deposit ranges between 60 HRC and 62 HRC and has a susceptibility for cold cracking. The layer shows excellent resistance against abrasion, moderate against impact, and moderate resistance against compression. This hardfacing material is used for earth moving industries, where abrasive wear caused by sand, minerals and earth occurs [Sol07].

Table 4.1: Chemical composition

	C	Si	Mn	P	S	Cr
Steel plate	0,18	0,19	0,67	0,021	0,028	-
Deposit layer	5	1,5	1,5	-	-	27

4.2 Equipment

4.2.1 Welding equipment

The power source is a "SAF Optipuls 350", which has a constant voltage characteristic. A conventional GMAW-welding gun (Profax 400 AMP) with 60° swivel goosenecks was used. Moreover, a welding tractor "Moggy GM-03-350", made by "Gullco", was used. The travel speed can be set in steps. The tractor is equipped with a permanent magnet on the bottom side.

4.2.2 Magnetic circuit

The experimental setup is given in figure 4.2. The magnetic yoke was connected to the welding tractor through an arm. The distance between the surface of a sample and the bottom side of the yoke was set to 10 mm in order to realize sufficient space between the deposit and the magnet. The distance between the two poles was limited due to the diameter of the welding gun. The magnetic field lines were parallel to the motion direction of the welding tractor in order to realize a longitudinal magnetic field. The welding gun was positioned at the center of the two poles. An illustration of this fact is given in figure 4.3.

The yoke was dismantled from a "Magnaflux" yoke and consists of various layers of thin steel plates to reduce the eddy effect. The magnetic flux density was measured with a

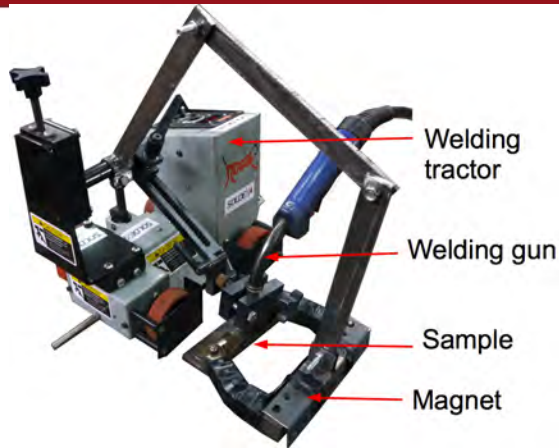


Figure 4.2: Experimental setup

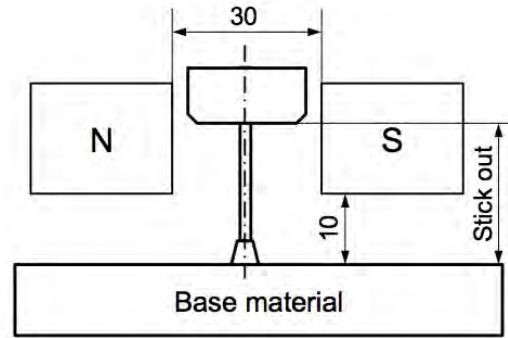


Figure 4.3: Schematic illustration of the position of the yoke and welding gun

magnetic flux meter in relation to the electric current in the spool and the set frequency at the point of interest. The initial measurements were carried on an experimental setup without welding gun and base material. The schematic setup is presented in figure 4.5.

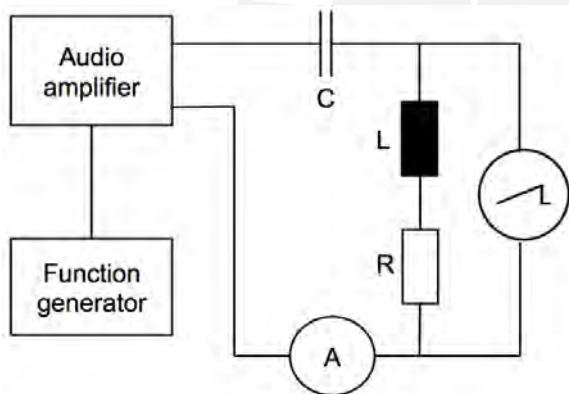


Figure 4.4: Schematic illustration of the electrical circuit

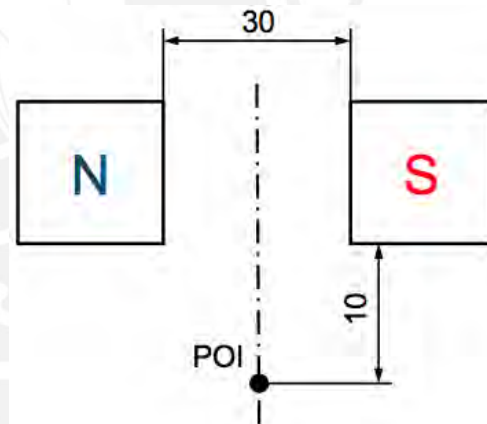


Figure 4.5: Schematic illustration of the position of the sensor of the tesla meter

As presented in figure 4.4, the signal of the function generator is amplified by a 100 W audio amplifier, representing constant voltage source. The electric current, voltage and the form of the signal were measured by a multimeter and an oscilloscope. The capacitor reduces the idle current within the circuit and was used for the frequency of 25 Hz and 45 Hz. For 25 Hz a capacitance of 60 μ F and for 45 Hz a capacitance of 20 F were used. The used equipment for the circuit is summarized in table 4.2.

Table 4.2: Equipment for the electric circuit

Equipment	Manufacture	Model number
Magnetic fluxmeter	F.W. Bell	4048
Osciloscop	Tektronix	TDS 340
Amplifier	TEAC	A-AX 5000
Function generator	Philips	PM 5131
Multimeter	EXTECH Instruments	380289

4.3 Processing

Two welds were deposited on each base plate. A schematic illustration of the dimensions is given in figure 4.8. Between two trails, the sample was cooled under air in order to realize similar process environments for the trails.

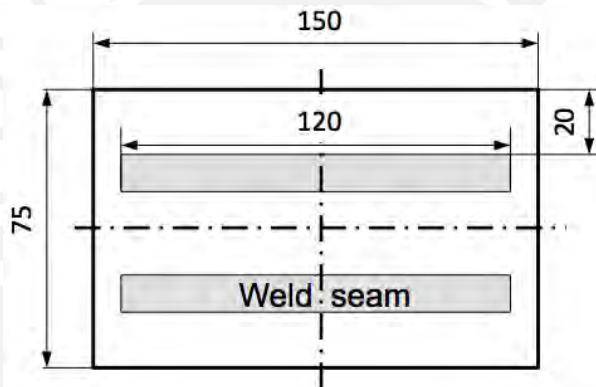


Figure 4.6: Dimension of the sample

The influence of the magnetic field was investigated using short circuit, pulsed and spray transfer mode. Furthermore, the influence of additional shielding gas (80 % Ar and 20 % CO₂) was analyzed for pulsed mode.

The frequency was varied between 2 Hz, 5 Hz, 25 Hz and 45 Hz and the magnetic flux density between 2 mT and 6 mT. A step of 4 mT was added for pulsed mode.

In order to determine the welding parameters, the recommendations of the supplier were used. Therefore, the stick out was set to 25 mm for short circuit welding. Wire feeding speed, voltage and travel speed were varied to realize a stable arc. The angle was set to 3° forehand welding, which realizes less penetration. The used parameters are presented in table 4.3.

Table 4.3: Welding parameters - short circuit

	v_{wire} [m/min]	U [V]	v_{travel} [cm/min]	Stick out [mm]	angle [°]	I [A]
Parameter set 1	4	24.1	30	25	-3	210
Parameter set 2	5.7	24.8	30	25	-3	260

The settings of pulse mode are summarized in table 4.4. The stick out had to be reduced, because working with magnetic oscillation led to unstable arc, even for low magnetic values. In order to weld with additional shielding gas, the voltage setting was higher.

Table 4.4: Welding parameters - pulsed mode

	Unit	Set1	Set2
v_{wire}	[m/min]	7.2	7.2
U	[V]	24.1	25
I_{peak}	[A]	400	400
I_{base}	[A]	80	80
f	[Hz]	240	240
pulse width	[ms]	2.9	2.9
v_{travel}	[cm/min]	30	30
Stick out	[mm]	18	18
angle	[°]	0	0
additional shielding gas		no	80%-Ar, 20%-CO ₂

The welding parameters for spray mode were determined in pretrails and are summarized in table 4.5. In order to stabilize the process, pure argon shielding gas was used.

Table 4.5: Welding parameters - spray mode

v_{wire}	U	v_{travel}	Stick out	angle	I
[m/min]	[V]	[cm/min]	[mm]	[°]	[A]
9.9	36.4	36	25	0	360

4.4 Engaged readings recorders

4.4.1 Video capturing

A conventional "Panasonic Lumix G5" camera, equipped with standard H-FS014042 lens, was used in order to take videos of the arc. A welding glass (DIN 169 - 6) and a grey filter (ND 0,9) were mounted in front of the lens. The camera was set to 60 frames per second with a resolution of 1920 x 1080 pixel. It was attached to the welding car to realize a constant distance between the camera and the arc.

The footage was analyzed in order to determine the influence of the magnetic values on the arc deflection. Therefore, the distance Δx between the the centerline of the wire and the deflected arc was measured. An illustration is given in figure 4.7.

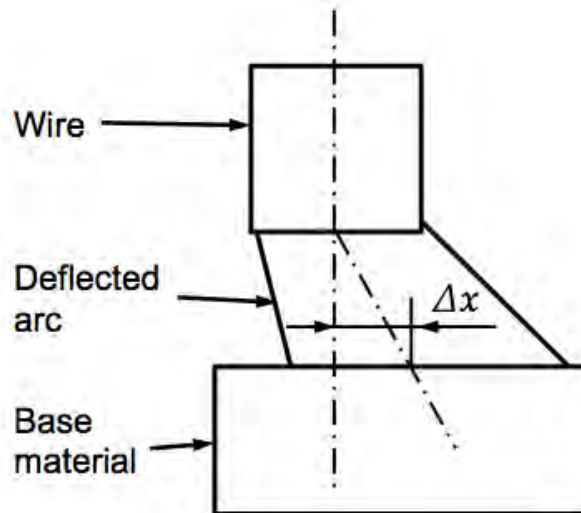


Figure 4.7: Distance between the centerline of the wire and deflected arc

4.4.2 Welding current

The welding current of the pulsed mode was measured with a "Fluke i1010" AC/DC current clamp. For short circuit mode a "Fluke 80i-400" AC clamp was used. The signal was captured with a "Tektronix TDS 2002B" oscilloscope.

4.5 Sample characterization

4.5.1 Metallography

The samples were cut with the manual cutting machine, model "Struers Labotom-3", followed by the metallography using "Buehler SimpliMet" mounting press and "Buehler TransOptic" powder (thermoplastic acrylic). After that manual grinding was carried out by using P150 to P1200 followed by manual polishing ($6\ \mu\text{m}$, $3\ \mu\text{m}$ and $1\ \mu\text{m}$). The samples were etched with a mixture of 60 mL HCl and 20 mL HNO_3 using the wipe technique. The cross section were examined with a "Leica DMI5000 M" microscope and Leica software.

Instead of the dilution area, the penetration depth p and the weld bead width w were determined using the "Leica 6D" stereo microscope. The reason for this is, that a reduced penetration depth and an increased width could led to the same area.

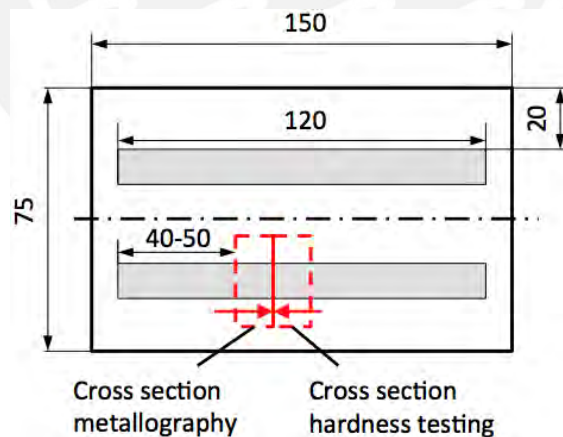


Figure 4.8: Schematic illustration of the dimensions of a sample

4.5.2 SEM analysis

SEM analysis was carried out in a few selected samples on a "FEI QUANTA 200" SEM to evaluate the chromium content using the EDX modus.

4.5.3 Hardness

For hardness testing, the surface of the samples was grinded up to the step of 1200P. A "Grayford Kent" hardness testing machine was used to measure the Vickers Hardness. The testing load was 20 kg. The measuring points were set according to figure 4.9. The average hardness was calculated from the measurement results within the deposit area.

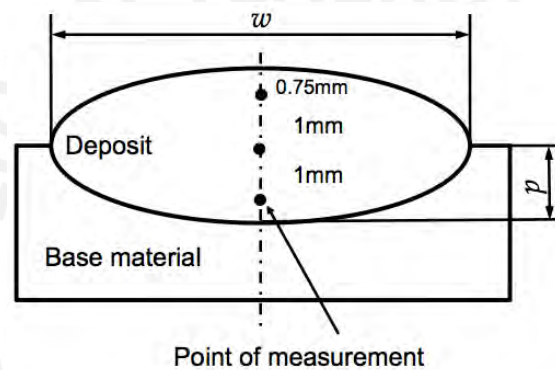


Figure 4.9: Schematic illustration of the hardness measuring points

5 Results and discussion

5.1 Magnetic circuit

In order to reduce the idle current, a capacitor was installed in the magnetic circuit for 25 Hz and 45 Hz. Therefore, the ohmic resistance of the spool was measured with 5.6Ω using a multimeter. For the electric circuit, a voltage of 35.52 V and current of 0.266 A at 50 Hz were measured. The inductance L was calculated with 0.4245 H.

Because it is not possible to determine the magnetic field density during the welding process, the relation of the electric current and the magnetic flux density for the circuit was measured. The results are illustrated in figure 5.1. An increase of the electric current is needed to realize the same value of magnetic flux densities for increasing frequencies. This can be explained with the increasing eddy effect for increasing frequencies.

The distribution of the magnetic flux density in relation to the distance from the centerline is given in figure 5.2. In a range of ± 3 mm the values vary between 6 mT and 6.18 mT.

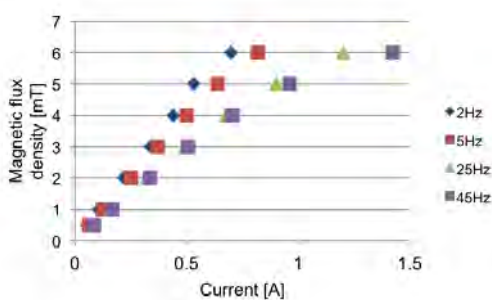


Figure 5.1: Schematic illustration of the dimensions of a sample

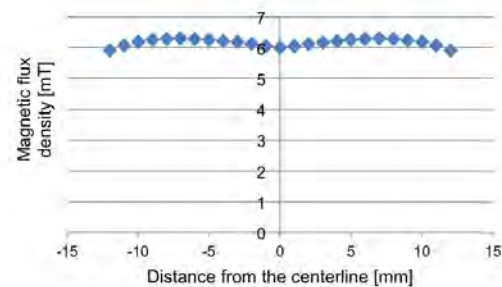


Figure 5.2: Distribution of the magnetic field density from the distance of the centerline

5.2 Welding results

5.2.1 Short circuit

5.2.1.1 Material transfer characteristics

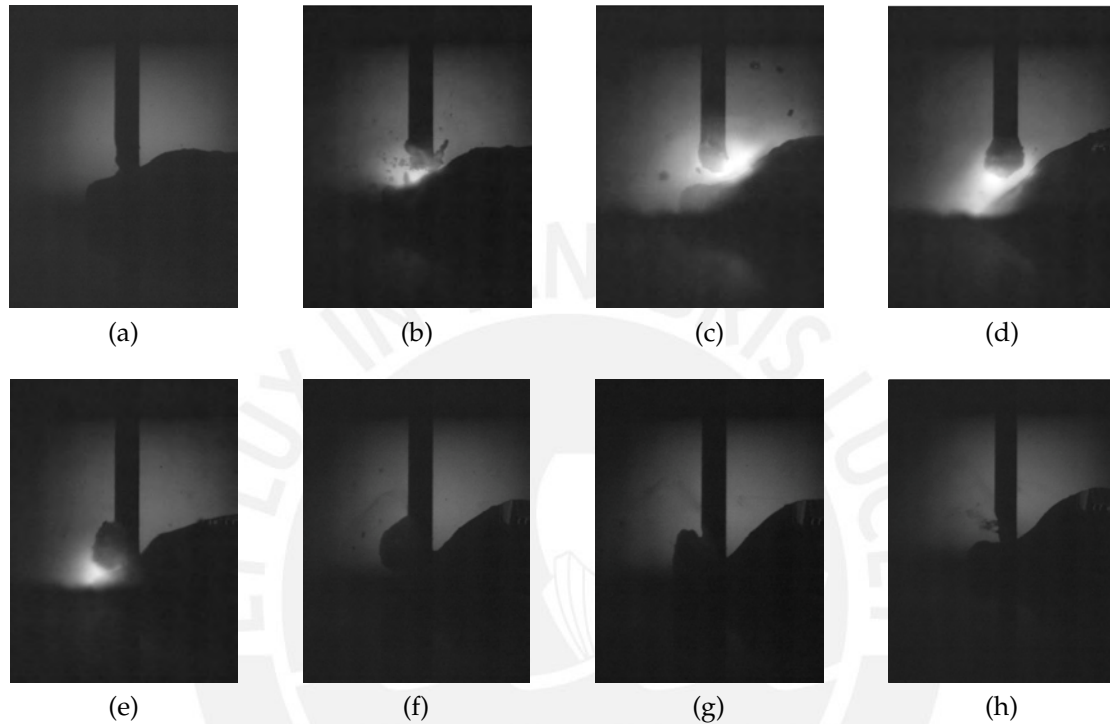


Figure 5.3: Material transfer during short circuit for FCAW [Kra]

The metal transfer in short circuit mode is presented in figure 5.3. The wire is fed into the superficial molten weld bead and causes a short circuit (see figure 5.3a and 5.3b). Due to the current of the short circuit and increased magnetic forces, the drop detaches the tip of the wire, an arc ignites and a partial melting of the wire occurs. A drop is formed (see figure 5.3d) and the arc is located between the drop and the molten substrate. The drop is fed into the molten weld bead due to continuous fed wire (see figure from 5.3f to 5.3h). The video footage from Kraußner [Kra] ¹ does not show an impact of the magnetic oscillation on the droplet size .

The influence of the magnetic field on the deflection can be observed in figure 5.4. The deflection using 6 mT is higher than for 2 mT. Using a frequency of 45 Hz, a high magnetic field has less impact on the deflection. A quantitative description of the

¹FCAW, 1.2 mm FeV12 electrode, shielding gas mixture: 96 % Ar, 3 % CO₂, 1 % O₂

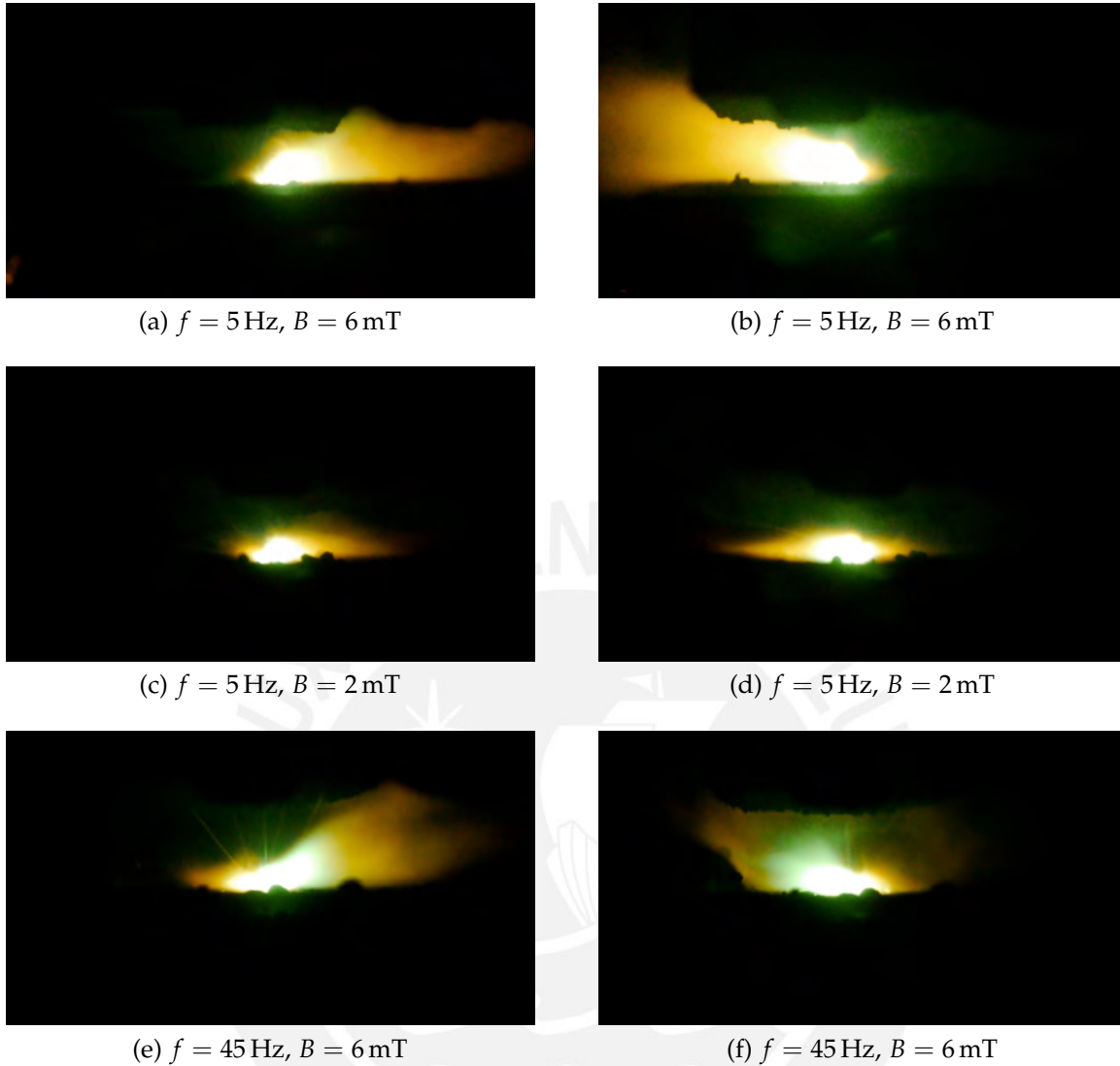


Figure 5.4: Comparison of arc deflection due magnetic oscillation

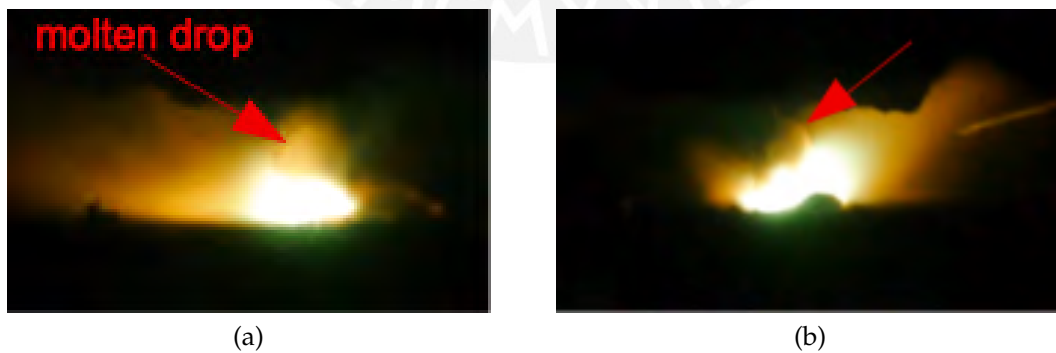


Figure 5.5: Characteristic drop formation, $f = 5 \text{ Hz}$ and $B = 6 \text{ mT}$

deflection caused by the oscillation is not feasible due to the provided equipment and the pulsed exposure. Further investigations with a high speed camera have to be carried out in order to quantitatively analyze the impact of the magnetic field on the deflection of the outer and inner plasma.

As it can be seen in figure 5.5 the drop forms on this side where the arc is deflected. This is the result of the Lorentz force, which acts on a current carrying conductor. This force moves the molten tip of the wire in the same direction, where the arc is deflected and an illustration is given in figure 5.6. Due to the process characteristics, the tip of the wire is fed into the molten weld bead. This explains the widening effect caused by the magnetic oscillation. An influence of a higher welding current on the deflection could not be observed. The current characteristics, which are presented in figure 5.7,

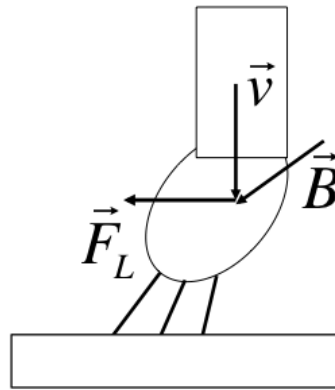


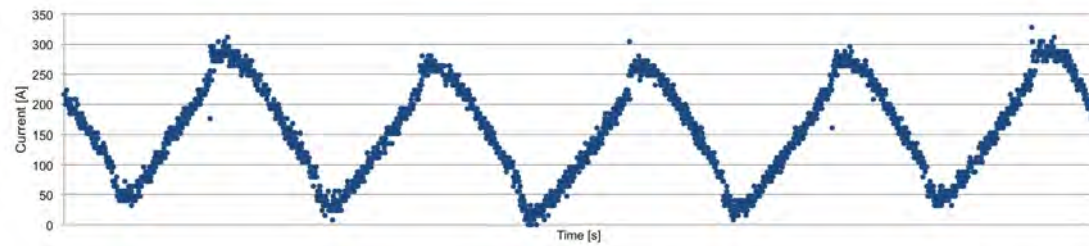
Figure 5.6: Acting Lorentz forces deflects the molten tip of the arc

exhibit differences in the steepness of the positive and negative slope. Without the magnetic field, the positive and negative slopes are similar. Applied magnetic field led to a steeper positive slope and a shallower negative slope. Furthermore, the peak of the characteristics is more flat and the peak-to-peak value is lower.

It is presumed, that the current is reduced due to the increased arc length and the power supply characteristics. Moreover, it reduces the time constant τ of the electrical circuit due to the increased resistance, which can be seen in the following equation.

$$\tau = \frac{L}{R} \quad (5.1)$$

This can explain the steeper positive slope. The flattened peak can be explained due to the power characteristics, which results in a current decrease during the deflection. Therefore, the concentric magnetic field, which contributes the droplet, is decreased as



(a) Without magnetic field

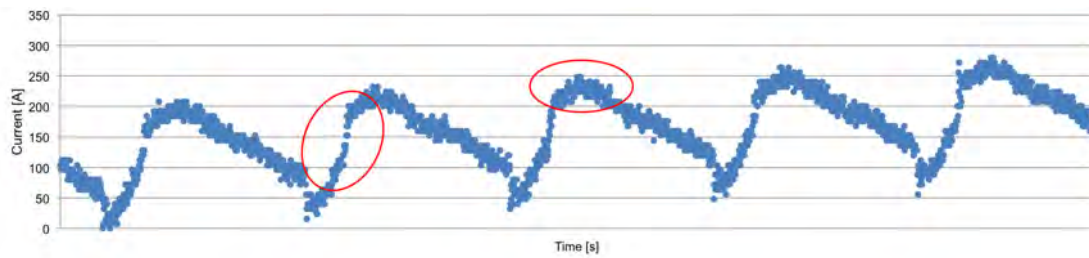
(b) $f = 5 \text{ Hz}$, $B = 6 \text{ mT}$

Figure 5.7: Impact of the magnetic field on the short circuiting arc current characteristic well and a longer time is necessary for the droplet detachment. Further investigations have to be carried out in order to investigate the relationship of the droplet detachment for short circuit process in an magnetic influenced environment.

5.2.1.2 Weld seam appearance

In general, the surface of the weld seam is rough and no solidification lines can be observed. Depending on the magnetic values, the weld seam appearance varies and each sample was assigned to three categories:

- good: no spatter and uniform weld seam appearance,
- acceptable: little spatter and unevenness,
- not acceptable: spatter and no uniform weld seam appearance.

For low magnetic values, the weld seam appearance is better than with high values. The results are summarized in table 5.1 and table 5.2. Examples of the seam appearance are given in figure 5.32.

Spatter was not observed for low and high magnetic fields. Transversal cracks (cold cracking) were observed in every weld and an example is given in figure 5.9. The amount of cracks in the weld was similar for all samples. Moreover, no slag was produced.

Table 5.1: Evaluation of the weld seam appearance

Frequency [Hz]	Magnetic flux density [mT]	
	2	6
2	+++	+++
5	+++	+++
25	+++	+++
45	+++	+++
+++	good	
++	acceptable	
+	not acceptable	

Table 5.2: Evaluation of the weld seam appearance

Frequency [Hz]	Magnetic flux density [mT]	
	2	6
2	+++	+
5	+++	++
25	+++	++
45	+++	+
+++	good	
++	acceptable	
+	not acceptable	



(a) $I = 210 \text{ A}$, $U = 24.1 \text{ V}$, $f = 45 \text{ Hz}$, $B = 2 \text{ mT}$



(b) $I = 260 \text{ A}$, $U = 24.8 \text{ V}$, $f = 45 \text{ Hz}$, $B = 2 \text{ mT}$



(c) $I = 260 \text{ A}$, $U = 24.8 \text{ V}$, $f = 45 \text{ Hz}$, $B = 6 \text{ mT}$

Figure 5.8: Influence of the magnetic field on the weld seam appearance

The weld seam appearance was not negatively influenced using magnetic field application under low voltage and electric current. That means, that the welding parameters were chosen right and the process window was not left.

In contrast to that, the weld seam was negatively influenced when using higher voltage and current. It is assumed, that a further optimization would have led to better results.

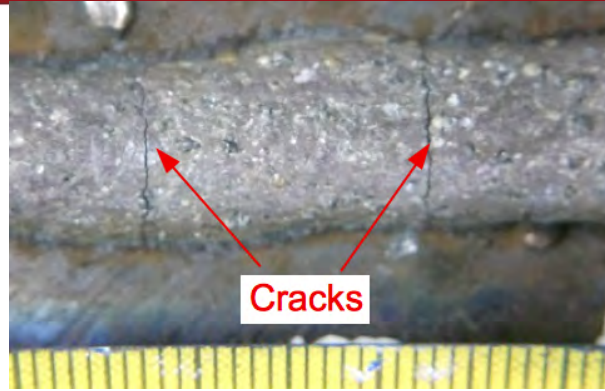


Figure 5.9: Transversal cracks in the weld seam

Working with a high magnetic field value leads to an excessive increase of the arc length, which can result in leaving the process window. The setting window for the power supply gets more narrow by increasing the magnetic field, respectively. This fact is illustrated in figure 5.10.

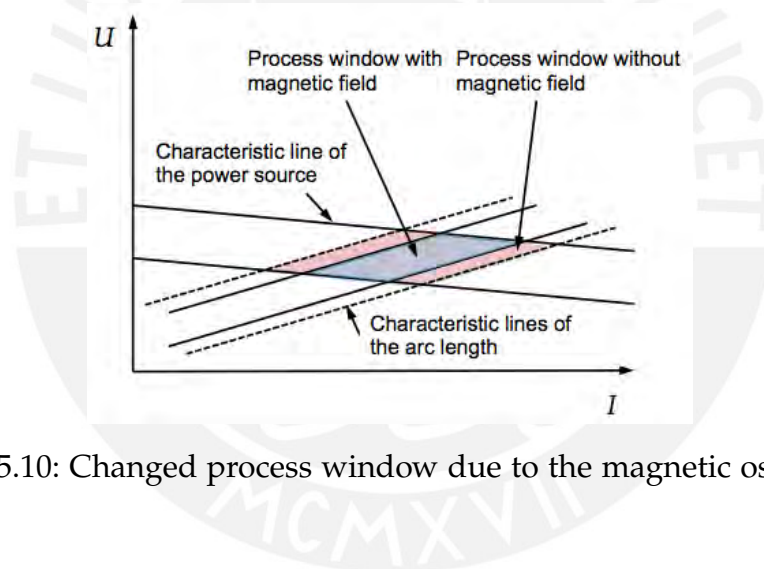


Figure 5.10: Changed process window due to the magnetic oscillation

5.2.1.3 Metallography

The influence of the magnetic field (frequency and magnetic flux density) on the penetration and weld bead width are presented in figure 5.11 for the lower welding setting parameters. Figure 5.12 shows the influence of the higher welding settings. Comparing the results from the energy input point of view, higher welding energy

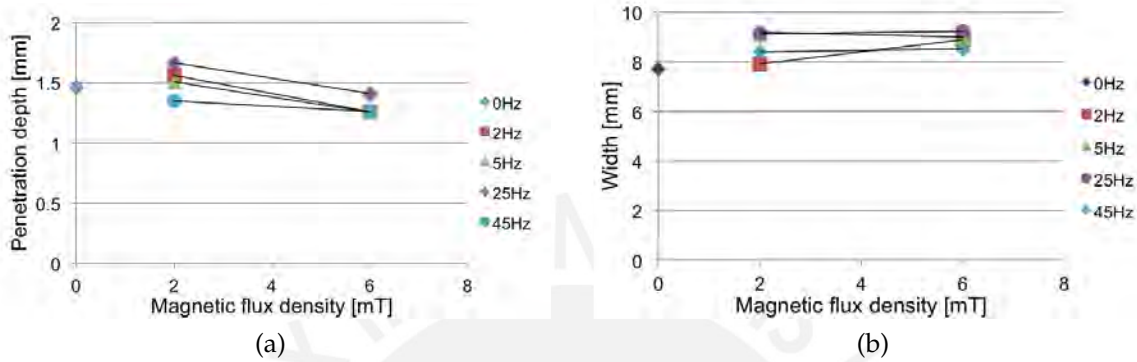


Figure 5.11: Influence of the magnetic field on the: (a) penetration depth and (b) width, $I = 210 \text{ A}$, $U = 24.1 \text{ V}$

lead to a higher penetration depth and a wider weld seam. The results of the lower welding parameter show, that the penetration is deeper at 2 mT in comparison to the weld without magnetic oscillation. Using 6 mT reduces the penetration. The lowest penetration depth was achieved with 6 mT and 2 Hz, 5 Hz and 45 Hz and a reduction of 14 % was obtained. The width is wider using a longitudinal magnetic field and increases slightly with increasing magnetic flux density. An improved width was achieved using 25 Hz and 6 mT, which means an increase of 17 %.

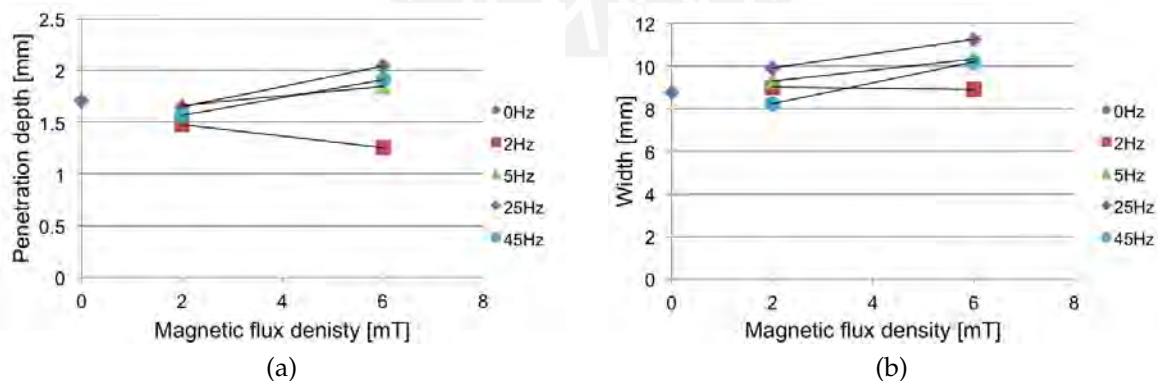


Figure 5.12: Influence of the magnetic field on the: (a) penetration and (b) width, $I = 260 \text{ A}$, $U = 24.8 \text{ V}$

A reduction of the penetration depth was only observed for a frequency of 2 Hz using magnetic oscillation and higher welding parameters. For the other pairs of values, the penetration increases by increasing the magnetic flux density. The seam gets wider, when the magnetic field is applied. An enhancement of 24 % was measured working with 25 Hz and 6 mT.

The effect of the magnetic field on weld penetration depth and width is clear and reasonable using lower welding settings. An increased magnetic field leads to less penetration depth and a wider bead. The weld width was increased with increasing magnetic flux density using higher welding values. However, it results in an increased penetration depth. Further investigations are necessary to explain this outcome.

The deflection results in an increased arc length, which causes a reduction of the welding current due to the power supply characteristics. This results in less heat input into the wire and the substrate and explains the reduction of the penetration depth.

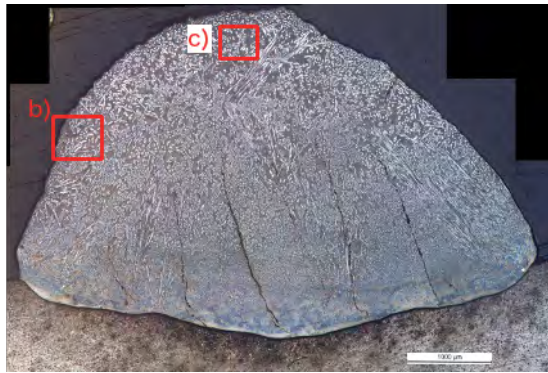
Two cross section are presented in figure 5.13. In the overview, longitudinal cracks can be observed, which are located at the bottom region of the seam. The chromium carbides of the type M_7C_3 distinguish themselves from the hypereutectic matrix. Their size decreases from the outer to the inner region, which can be observed in figure 5.12b. Moreover, the carbide size decreases from the top to the bottom side. An influence of the magnetic field on the microstructure was not determined (see figure 5.13 and 5.14).

5.2.1.4 SEM analysis

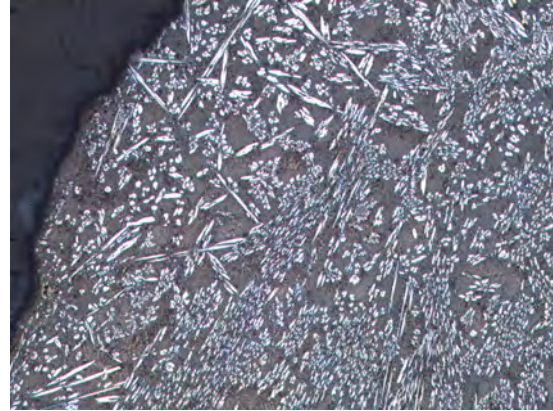
Figure 5.15 shows an image of the SEM analysis. The dark toned areas represent the chromium carbides and the bright areas the matrix. EDX analysis revealed a chromium content of 33 % in the dark toned area and 15 % in the bright region. The rest is indicated as iron for both areas.

5.2.1.5 Hardness

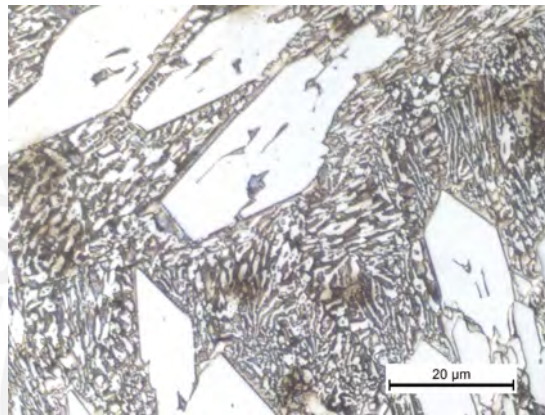
The results of the hardness testing, which are presented in figure 5.16, show an increased hardness of 50 HV for the frequency of 2 Hz and 6 mT in comparison to the control sample. The other results are located in one range of variation and vary between $651 \text{ HV} \pm 14 \text{ HV}$ and $691 \text{ HV} \pm 5 \text{ HV}$.



(a) Overall view

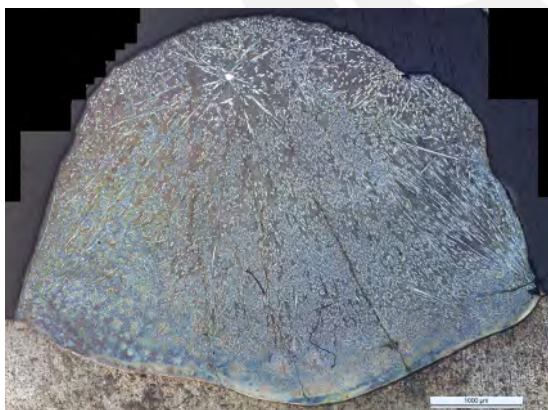


(b) Detail view at 50x

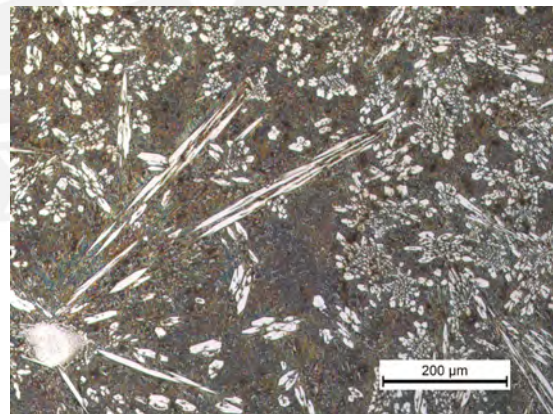


(c) Detail view at 1000x at top area

Figure 5.13: Cross section of sample D17, $I = 260 \text{ A}$, $U = 24.8 \text{ V}$, $f = 2 \text{ Hz}$, $B = 6 \text{ mT}$



(a) Overall view



(b) Detail view at 50x

Figure 5.14: Cross section of the control sample, $I = 260 \text{ A}$, $U = 24.8 \text{ V}$, no magnetic field

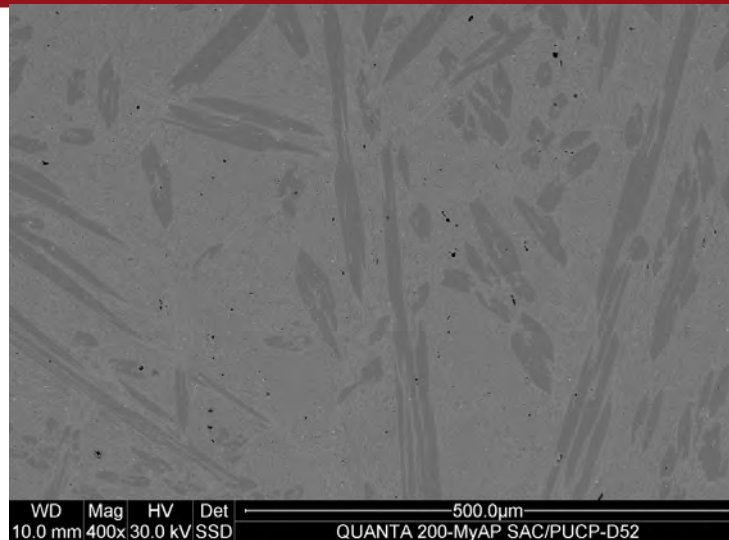
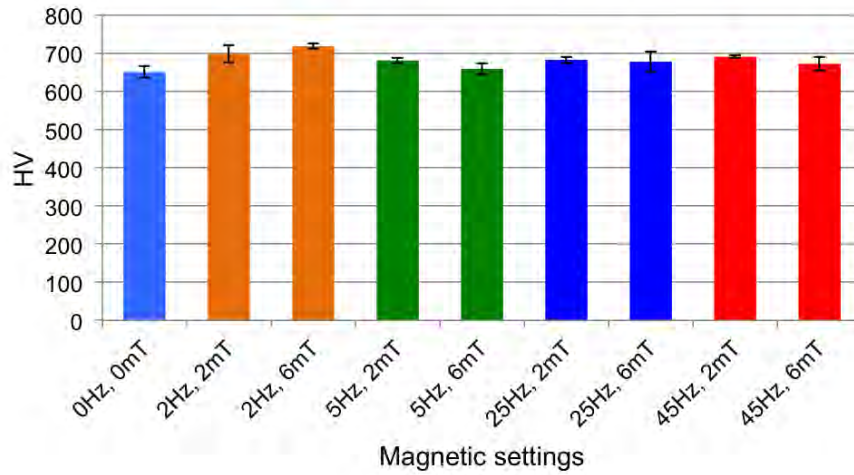


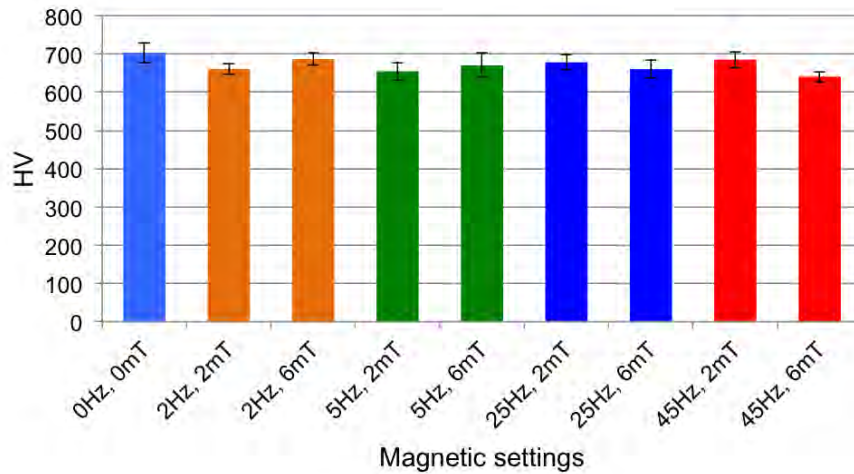
Figure 5.15: SEM analysis of sample D51, $I = 260$ A, $U = 24.8$ V, $f = 5$ Hz, $B = 6$ mT

Considering the hardness results of samples produced with higher energy welding, all average values are located in a variation range (see figure 5.16b). The maximum hardness was measured with $703 \text{ HV} \pm 26 \text{ HV}$ (control sample) and the lowest with $640 \text{ HV} \pm 13 \text{ HV}$ ($f = 45$ Hz and $B = 6$ mT).

The hardness results range in a spectrum between 650 HV and 700 HV of both welding settings. The supplier specified a hardness range from 60HRC to 62HRC for the third layer deposit. The converted value vary between 697 HV to 745 HV. Considering that one layer was produced and measured, the values are good. It can be presumed, that carbon diffused into the base material due dilution and therefore, the measured values are lower.



(a) $I = 210 \text{ A}$, $U = 24.1 \text{ V}$



(b) $I = 260 \text{ A}$, $U = 24.8 \text{ V}$

Figure 5.16: Influence of the magnetic field on the hardness, short circuit

5.2.2 Pulsed transfer mode

5.2.2.1 Material transfer characteristics

Figure 5.17 illustrates the material transfer during pulsed mode and the characteristic droplet detachment from the tip of the wire can be observed. One droplet forms and detaches from the tip of the wire during the peak current phase (see figure 5.17a and 5.17b). The bright area in figure 5.17b represents the arc during the high current phase, followed by the low current phase, where the droplet falls into the molten weld bead while the arc is still present. This can be observed in figure 5.17c. In the next figure

5.18, the deflection of the arc by the magnetic field oscillation can be seen clearly as well as the release direction of molten droplet (see figure 5.18c).

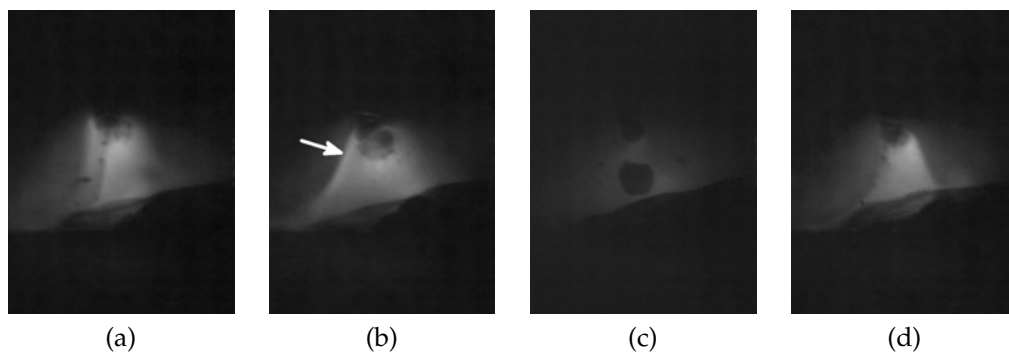


Figure 5.17: Material transfer during pulsed mode for FCAW [Kra]

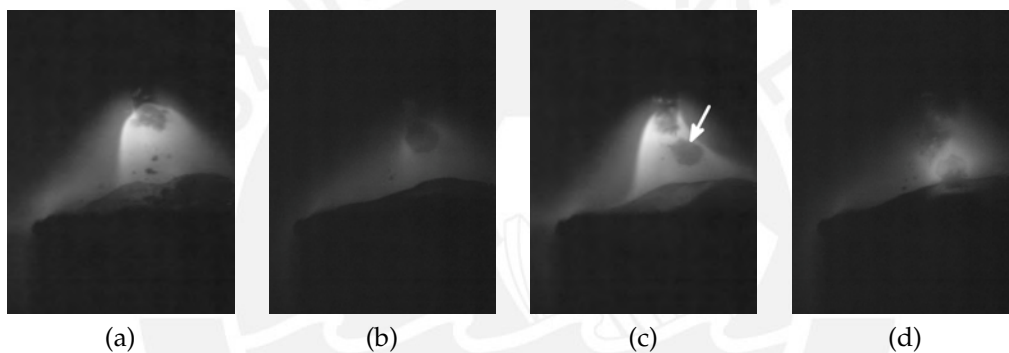


Figure 5.18: Material transfer during pulsed mode for FCAW with magnetic oscillation, $f = 20 \text{ Hz}$, $B = 5 \text{ mT}$ [Kra]

Increasing the magnetic flux density leads to a higher deflection of the outer arc, which can be observed in figure 5.19. Examples of the deflection are presented in figure 5.21. The deflection increases linear with increased magnetic flux density. The slope is higher for 2 Hz in comparison to 5 Hz and 25 Hz. The slope for 45 Hz is the lowest.

The high speed camera footage from Krauß [Kra] shows an uneven droplet detachment for high magnetic flux densities. The melting tip of the wire starts to form a drop and is deflected. The drop starts to grow and releases itself much later in comparison to the control sample. Moreover, droplets were identified, which did not fall off into the liquid weld bead (spatter).

The impact of the oscillation system on the pulsed arc current characteristic is illustrated in figure 5.21. The typical positive and negative slopes of the current for this type of

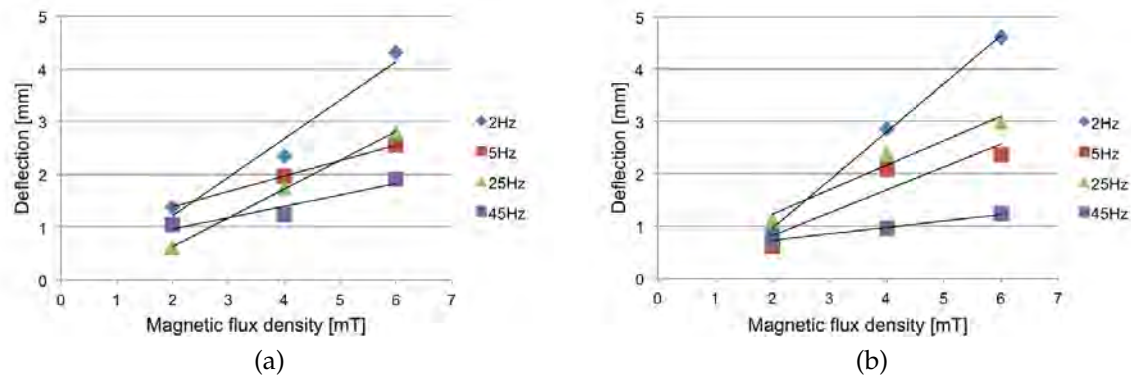


Figure 5.19: Influence of the magnetic field density and frequency on the arc deflection(a) without additional shielding gas (b) with additional shielding gas

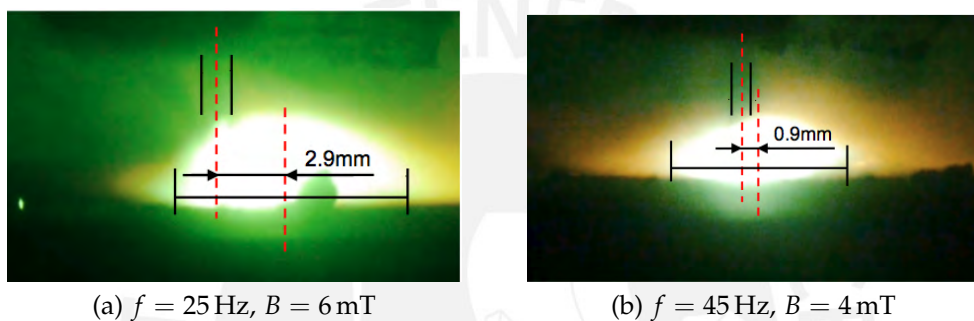
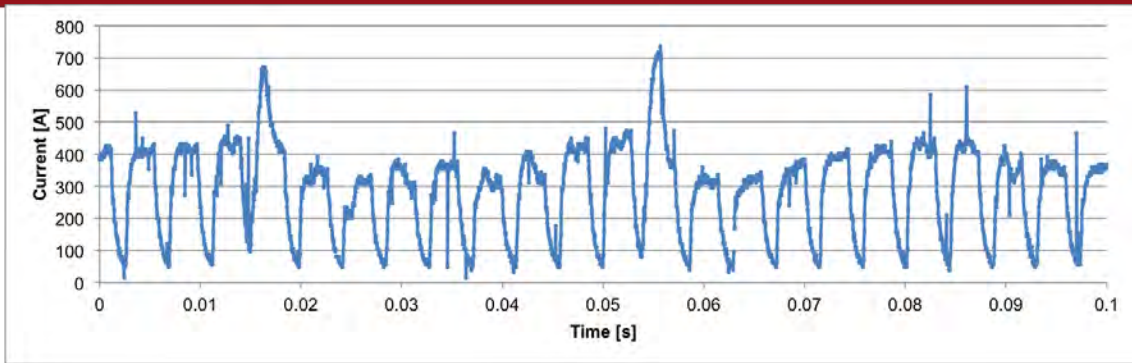


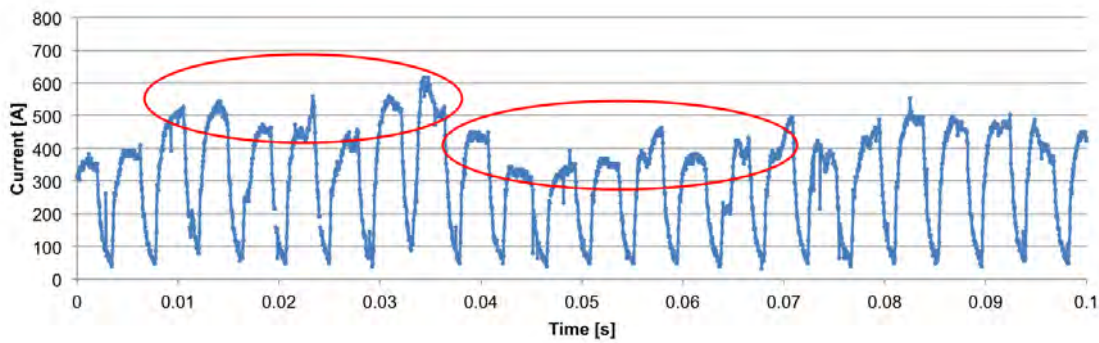
Figure 5.20: Deflection of the arc during pulsed mode, with additional shielding gas

welding power source can be encountered as well. Observing the current characteristics with applied magnetic field (figure 5.21b), the peak current in the range from 0.01 s to 0.03 s and in the range from 0.08 s to 0.1 s is higher than the peak current in the range from 0.04 s to 0.07 s. The trend of the various peaks shows a slight tendency, that two oscillation peaks of the magnetic field are superimposing the pulses. In order to draw reliable conclusions and distinguish the magnetic field impact and the stray area of the pulse amplitudes, it is necessary to record a longer time span.

The external magnetic field causes a change of the radial symmetrical acting forces on the drop into asymmetrical. Moreover, the plane of the acting forces turns, because the Lorentz force deflects the droplet and therefore changes the current of the electrons. This is illustrated in figure 5.22. As a result, the releasing droplet receives a transversal acceleration and gets deflected. The footage shows, that the drop size increases with high magnetic field in deflected position and droplets do not detach during the pulse. The control unit increases the peak current in order to stabilize the process, which was observed in the current characteristic. It can be assumed, that the power supply reaches



(a) Without magnetic field



(b) $f = 25 \text{ Hz}$, $B = 2 \text{ mT}$

Figure 5.21: Impact of the magnetic field on the pulsed circuiting arc current characteristic

its limit and therefore the droplet size increases. Because the electric current is too low, an equilibrium of the forces is caused resulting in an aggravated droplet detachment.

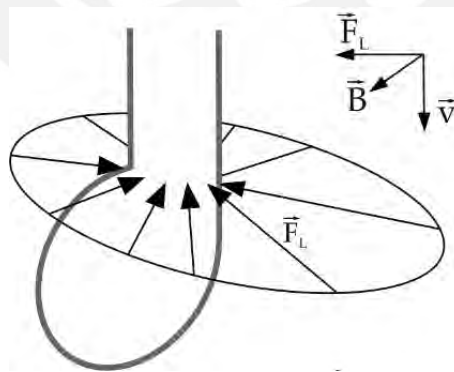
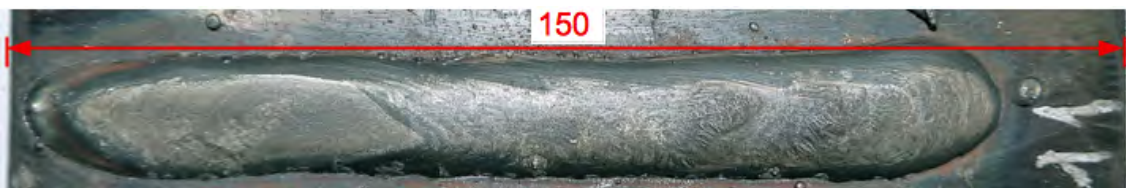


Figure 5.22: Changed Lorentz force acting on the droplet

5.2.2.2 Weld seam appearance

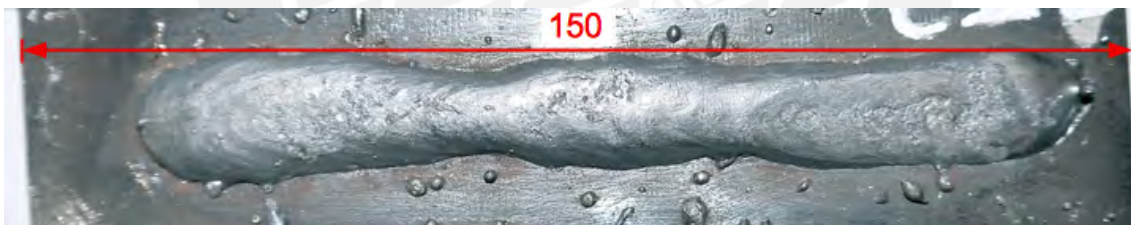
Observing the samples with the use of additional shielding gas, the weld appears smooth and more oval compared to the weld using short circuit. Transversal cracks were determined in all samples. Due to the magnetic field, the weld seam appearance changes depending on the magnetic settings. For low frequencies, no negative impact on the look of the seam was noticed. Spatter and uneven weld bead appearance occurred for frequencies above 25 Hz. The results are summarized in table 5.3 and examples are given in figure 5.23.



(a) $f = 2$ Hz and $B = 4$ mT, good appearance



(b) $f = 5$ Hz and $B = 6$ mT, acceptable appearance



(c) $f = 25$ Hz and $B = 6$ mT, not acceptable appearance

Figure 5.23: Weld seam appearance for pulsed mode with additional shielding gas

In contrast to that, no spatter and inhomogenous seam appearance due to oscillation occurred working with the self shielding process. A little uneven appearance for frequencies above 25 Hz was observed. The results are summarized in table 5.4 and example are given in figure 5.24. The surface of the weld is rough, like in short circuit mode and transversal cracking (cold cracking) was observed as well.

In contrast to the self shielding process, the longitudinal magnetic field led to spatter and uneven weld seam appearance when working with additional gas. Probably, turbulences are induced to the oscillation, which caused an unstable welding process

Table 5.3: Evaluation of the weld seam appearance, pulsed mode with additional shielding gas

Frequency [Hz]	Magnetic flux density [mT]		
	2	4	6
2	+++	+++	++
5	+++	+++	++
25	+++	++	+
45	+	+	+
+++	good		
++	acceptable		
+	not acceptable		

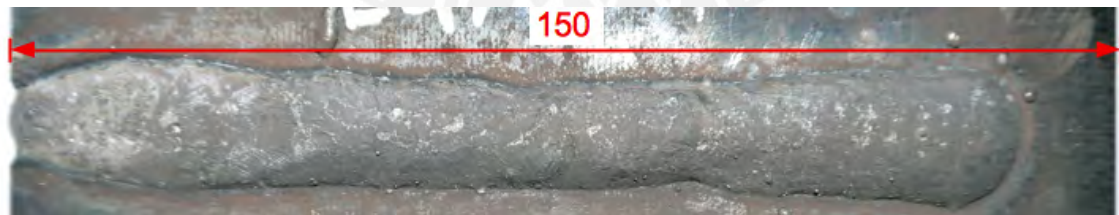
Table 5.4: Evaluation of the weld seam appearance, self shielded pulsed mode

Frequency [Hz]	Magnetic flux density [mT]		
	2	4	6
2	+++	+++	+++
5	+++	+++	+++
25	+++	+++	++
45	+++	+++	++
+++	good		
++	acceptable		
+	not acceptable		

especially for frequencies above 25 Hz. Due to turbulences a change of the acting forces on the droplet occurs as well as atmospheric gases influences the arc. Moreover, this can explain the lower effect of magnetic field on the arc deflection at higher frequency. Further investigations have to be carried out using a more sufficient camera. As well, the internal control of the power source can suppress further effects.



(a) No magnetic oscillation



(b) $f = 45 \text{ Hz}$ and $B = 6 \text{ mT}$

Figure 5.24: Weld seam appearance for pulsed mode, self shielding process

5.2.2.3 Metallography

The impact of the oscillation on penetration and width using additional shielding gas is presented in figure 5.25. A reduction of the penetration depth can be achieved with a frequency of 2 Hz and 5 Hz. The depth decreases with increasing magnetic flux density. The results regarding the frequency of 25 Hz and 45 Hz are higher than the results of the control samples. The lowest penetration depth of 1.6 mm was determined using 2 Hz and 4 mT (reduction of 38 %) and the deepest of 3.15 mm using 25 Hz and 6 mT. A widening of the seam can be achieved using 2 Hz, 5 Hz and 25 Hz and 2 mT and 4 mT. The maximum width was achieved with 2 Hz and 4 mT and amounts an increase of 21 % compared to the control sample. The results using the settings of 45 Hz have to be estimated with caution, because of the uneven weld seam appearance caused by the unstable arc.

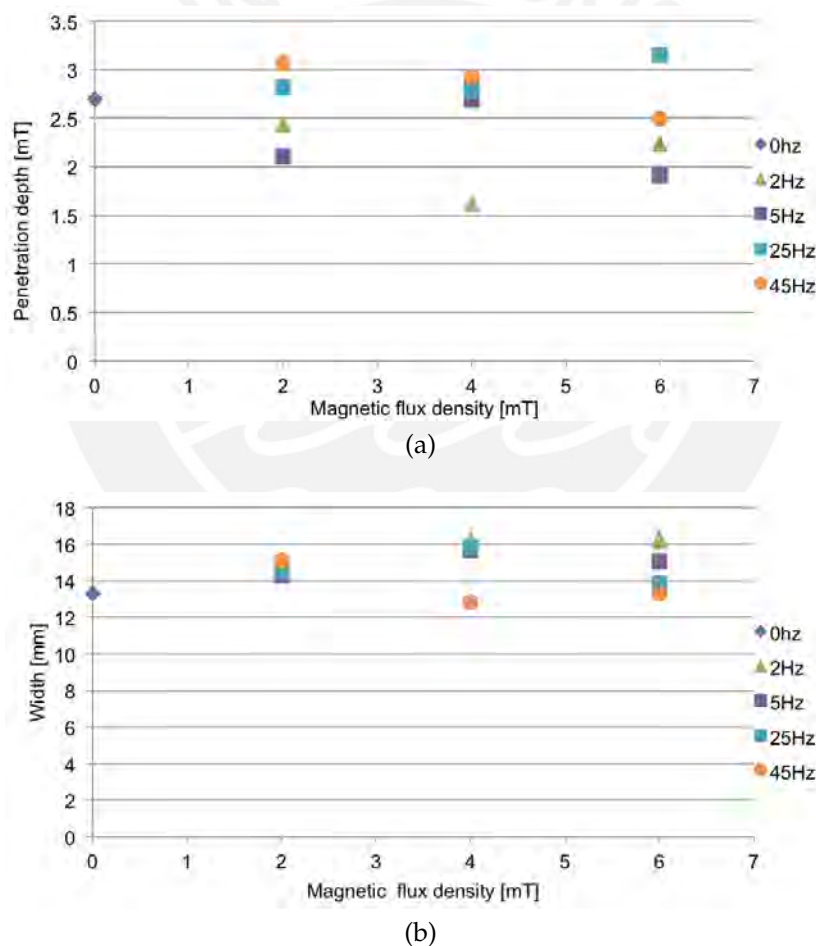


Figure 5.25: Influence of the magnetic field on the (a) penetration depth and (b) width, with additional shielding gas

The relationship of magnetic settings on seam dimensions for the self shielding process is given in figure 5.26. A reduction of the penetration can only be observed for a frequency of 5 Hz. A defined impact of the magnetic setting ($f = 2\text{ Hz}$, 25 Hz and 45 Hz) on the penetration depth cannot be identified. The width increases using 2 Hz and 5 Hz and 2 mT and 4 mT . The maximum width of 16.3 mm was achieved using 2 Hz and 6 mT , which is an increase of 19% compared the control sample. A reduction of the width can be noticed with increasing magnetic flux density for a frequency of 25 Hz and 45 Hz .

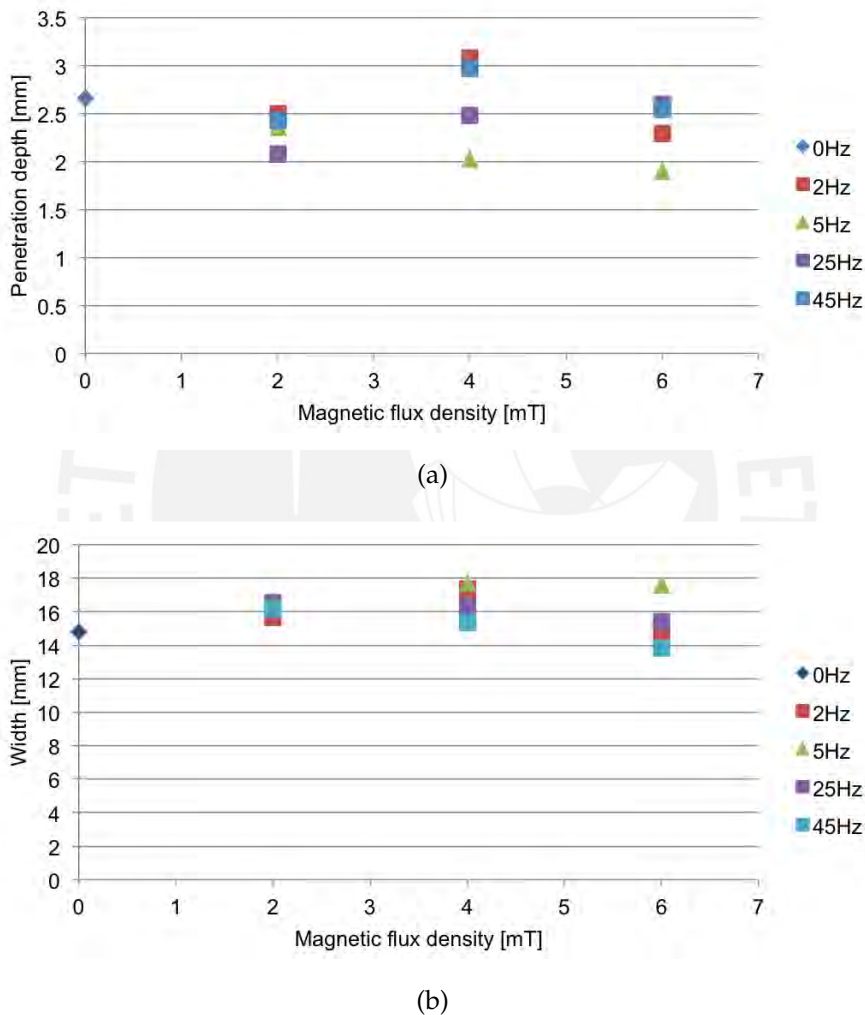


Figure 5.26: Influence of the magnetic field on the (a) penetration depth and (b) width, self shielding

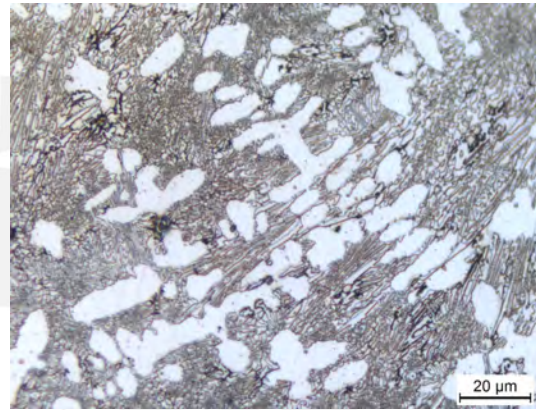
The results of the weld seam inspection can be transferred to the results of the weld bead dimensions. The tendency of decreased penetration and increased width with increasing magnetic field is demonstrated for low frequencies. Due to the lack of arc control, the results do not achieve the expected value at higher frequencies.



(a) Overview



(b) 50x, detail view



(c) 500x, detail view

Figure 5.27: Cross section of sample E27; $f = 25$ Hz and $B = 4$ mT

One example of the cross section is presented in figure 5.27. Due to the higher wire feeding rate, the weld seam width is up to two times wider in comparison to the width of the short circuit samples. The shape is more oval and a higher penetration depth can be noticed. In contrast to short circuit transfer mode, the cross section do not show the presents of chromium carbides. Dendrites are located in the eutectic matrix.

5.2.2.4 SEM analysis

Figure 5.28 shows an image of the SEM analysis. The bright appearing dendrites are located in the darker matrix. The EDX analysis revealed a chromium content of 11 % in the dendrites and 16 % in the matrix. The rest is indicated as iron for both areas.

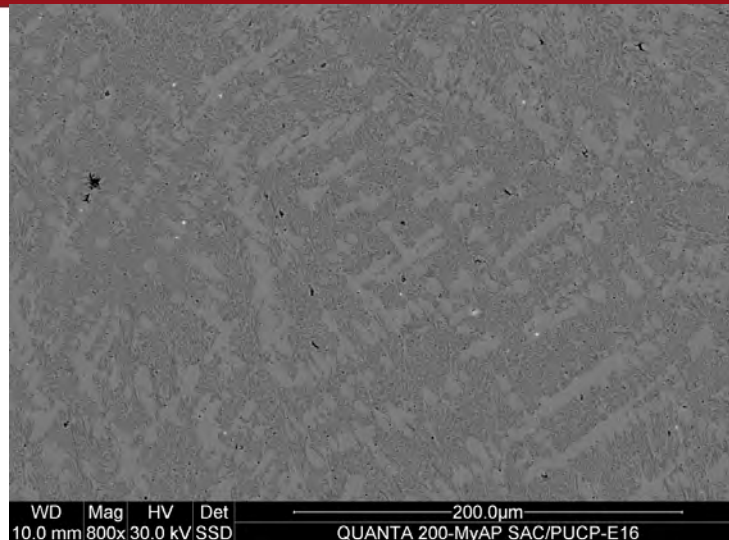


Figure 5.28: SEM analysis sample E16; $f = 45$ Hz and $B = 6$ mT

5.2.2.5 Hardness

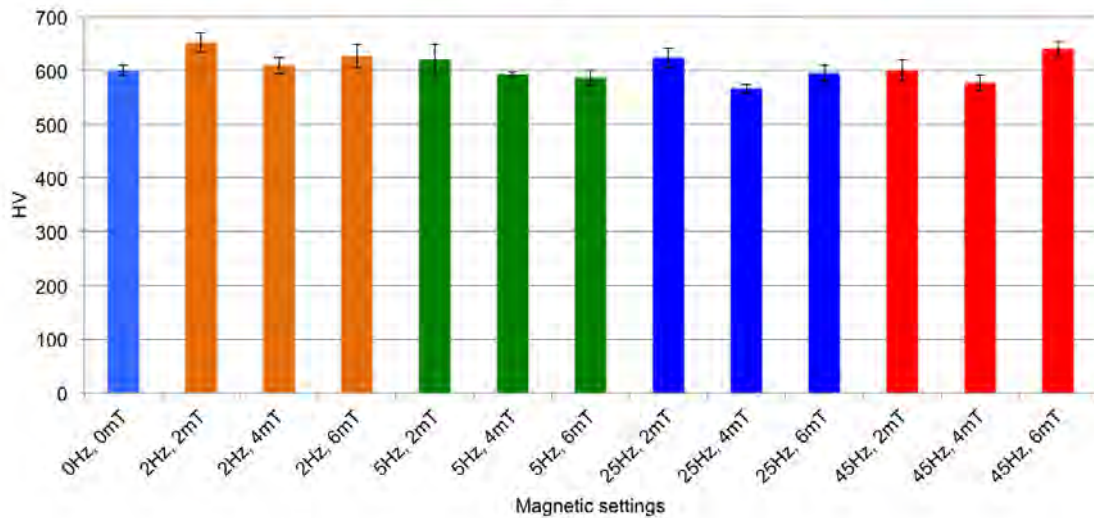
Based on the bar diagrams (see figure 5.29), no influence of the magnetic field on the hardness can be determined. The averages of the hardness values for all settings are in one range of variation. The lowest hardness of $566 \text{ HV} \pm 8 \text{ HV}$ was determined using 25 Hz and 4 mT and the highest hardness of $651 \text{ HV} \pm 18 \text{ HV}$ was measured working with 2 Hz and 2 mT. The average hardness for pulsed mode is lower than for short circuit.

5.2.3 Spray mode

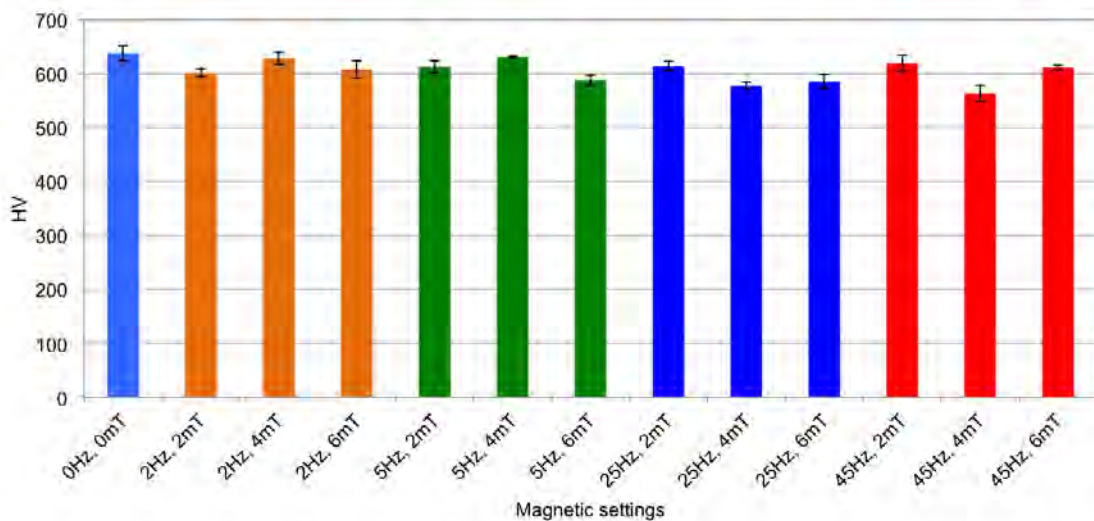
5.2.3.1 Material transfer characteristics

The characteristic material transfer of the spray mode is given in figure 5.30. The arc burns between the tip of the wire and the base material. Because of the heat, the tip of the wire is plasticized and a droplet forms. The droplet grows, is constricted due to the magnetic forces and gets detached from the wire. Eventually, the droplet falls into the liquid weld bead. Parts of the filler material fall out of the open wire into the weld bead.

The video footage working with 10 Hz and 10 mT shows the effect of the oscillation on the arc deflection and droplet detachment. An increase of the droplet size and a



(a) With additional shielding gas



(b) Self shielding method

Figure 5.29: Influence of LMF on hardness, pulsed mode

change of the release direction can be observed. Moreover, a decrease of the droplet detachment frequency was noticed.

5.2.3.2 Weld bead appearance

Due to the application of the magnetic field, even with a low magnetic flux density of 2 mT, spatter occurred and arc instability was noticed. The shape of the weld seam is not uniform and rest of the wire is located next to the seam. The arc became more unstable when applying a magnetic flux density of 4 mT.

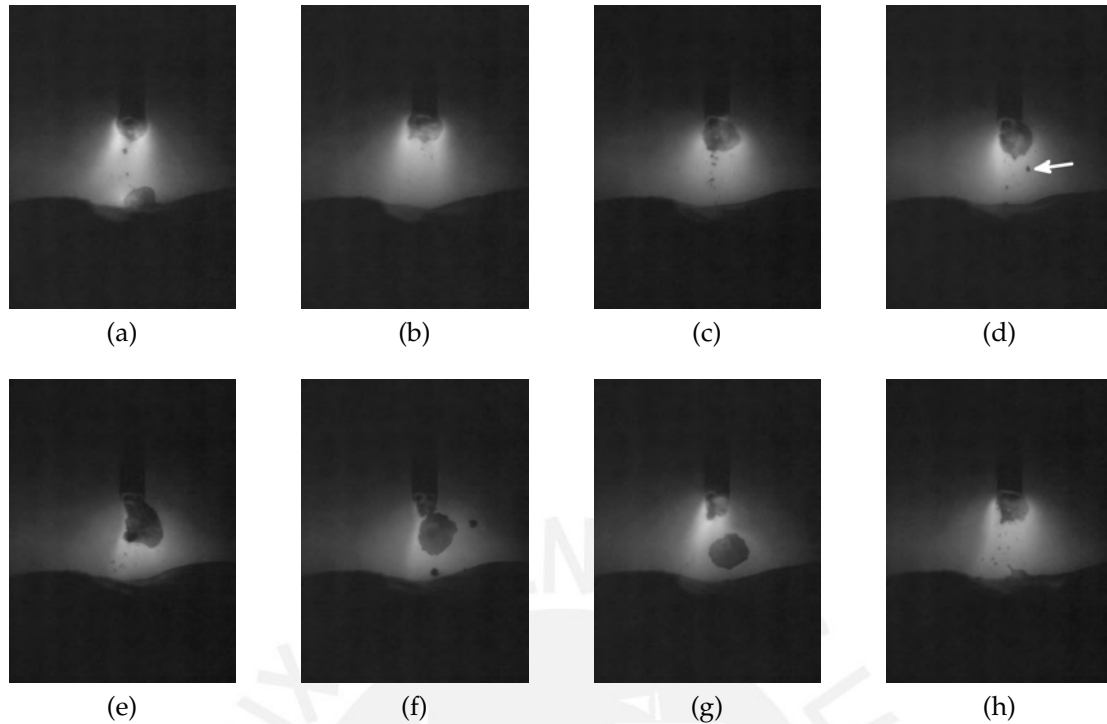


Figure 5.30: Material transfer during spray mode for FCAW [Kra]

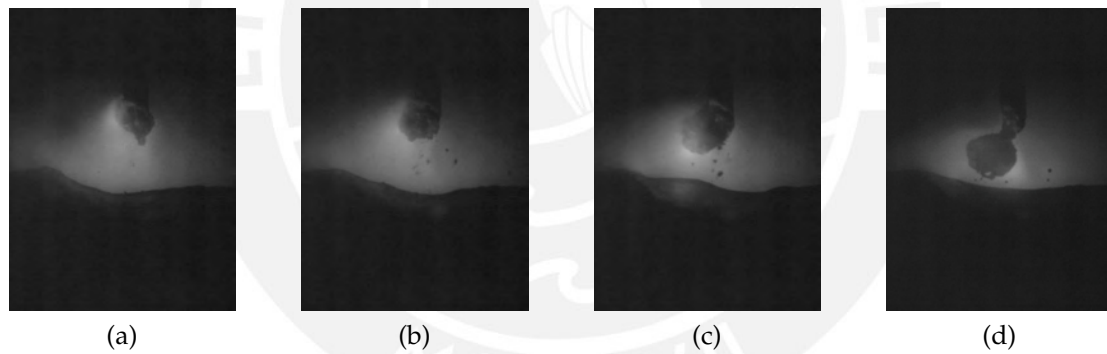


Figure 5.31: Material transfer during spray mode for FCAW, $f = 10 \text{ Hz}$ and $B = 10 \text{ mT}$, [Kra]

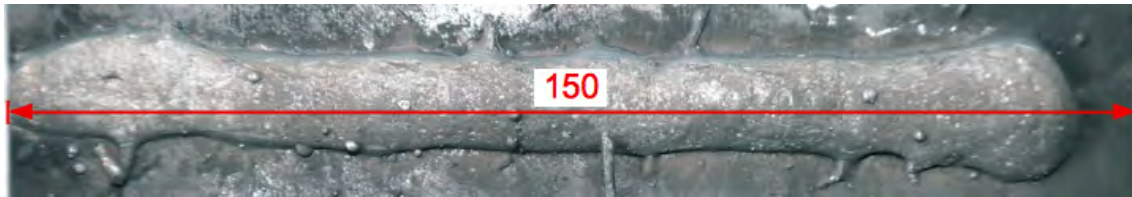
The penetration is higher in spray mode in comparison to the other transfer modes and an example is given in figure 5.33. Therefore, no further investigations were carried out, because the high penetration does not fulfill the requirements for a hardfacing application and the tendency, that an improvement of the weld bead due magnetic field is not feasible when using this wire.

It has to be pointed out, that this electrode has self shielding characteristics. It is not possible to define the gas mixture, which results from the external pure argon gas and

the self produced CO₂. It can be presumed, that the share of each shielding element within the mixture is varying for different points of the arc. An applied external magnetic field results in lack of arc control, even for low magnetic fields.



(a) Without external magnetic field



(b) $f = 2 \text{ Hz}$, $B = 2 \text{ mT}$



(c) $f = 45 \text{ Hz}$, $B = 4 \text{ mT}$

Figure 5.32: Influence of the magnetic field on the weld seam appearance, spray mode

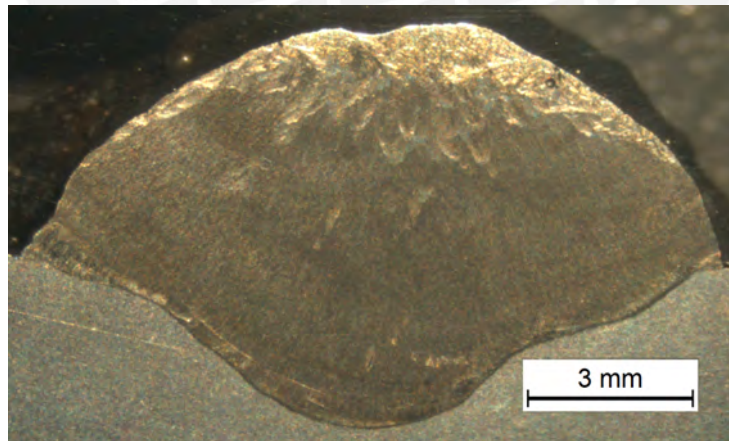
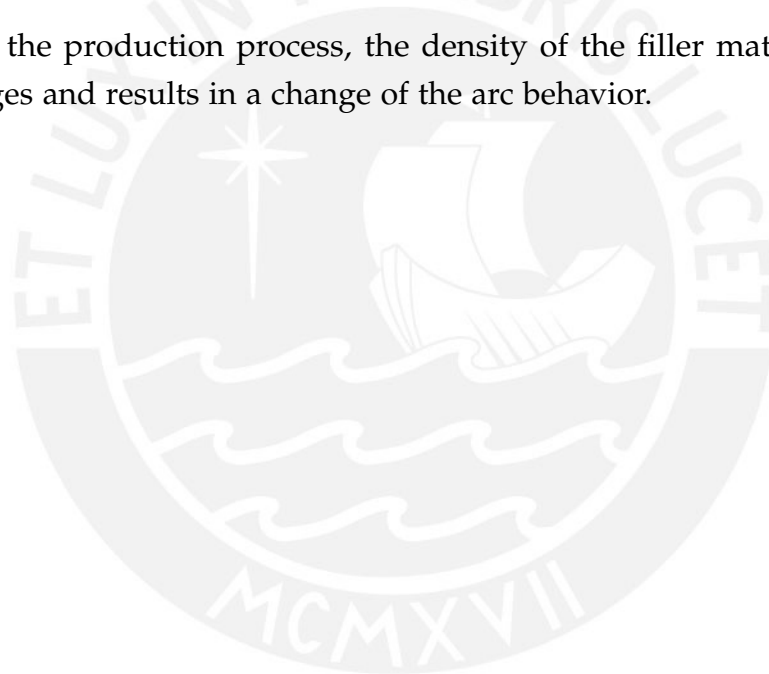


Figure 5.33: Cross section, spray mode, $f = 2 \text{ Hz}$, $B = 2 \text{ mT}$

5.3 Error consideration

Several factors have to be considered, which influenced the results negatively. First of all, the magnet and the welding gun were positioned manually, which influenced the reproducibility. Moreover, the results are influenced by the friction between the liner and the wire, which has an impact on the wire feeding speed and therefore on the welding process. The magnetic field interacts with the samples and welding table, which caused mechanical vibrations of the yoke and the welding gun. This was minimized by design, but not neutralized. The poles of the yoke were heated up in consequence of the welding process. This results in a increase of the magnetic resistance and a reduction of the magnetic field density. The current in the coil was set indirectly due to the audio amplifier, which acts as a voltage supply. A temperature change of the cable leads to a change of the cable resistance and to a change of the current.

As a reason of the production process, the density of the filler material within the electrode changes and results in a change of the arc behavior.



6 Summary

The objective of this thesis was to investigate the influence of a transversal magnetic field on the FCAW process. Therefore, a magnetic system was set up and characterized. In general, the arc can be manipulated during short circuit, pulse and spray transfer mode. Nevertheless, the results of the investigations show, that considerations have to be taken in order to receive a good weld bead appearance on one hand and on the other hand to take advantage of the magnetic system.

For short circuit welding, an increase of the weld bead width of 24% was achieved when applying the magnetic field. The reason for the changed weld shape dimension is, that the molten tip of the wire is deflected due to the acting Lorentz force. Because of the increasing arc length and the power supply characteristics, the process window gets more narrow and therefore, the welding parameters have to be selected with applied magnetic field. The impact of the system on the weld bead is more distinctive for pulsed and spray transfer mode, because the detached droplet can be manipulated in their trajectory. An widening of the seam of 20% and a reduction of the penetration depth of 30% was achieved using the pulsed open arc process. For the pulsed mode process, the use of additional shielding gas and high deflection frequencies led to a lack of arc control, probably due to turbulences. Moreover, the application of arc deflection on the spray mode cannot be recommended for the type of electrode used in this investigation.

An impact of the magnetic field on the microstructure was not determined. Due to higher welding energy at pulsed mode, the kinetic thermodynamical conditions were changed and hence, the formation of carbides did not occur. Therefore, the hardness was reduced for pulsed mode in comparison to short circuit mode.

7 Outlook

The investigation shows the potential to combine the advantages of the flux cored arc welding and the deflection of the arc due to magnetic fields. Further investigations have to be carried out to verify the drawn conclusions and to understand further characteristics of the process.

The use of a constant current source for the magnetic circuit represents an optimization. Furthermore, a modification of the welding power source in order to increase the current during the deflection, can realize a constant heat input into the wire. Moreover, the use of a free programmable welding power source can establish the understanding of the droplet detachment during pulsed mode and applied magnetic field. Because the influence of the magnetic field on the material transfer for self shielding flux cored arc welding was not investigated with a high speed camera, further investigations are necessary. Moreover, it is necessary to determine the effect of the magnetic field on the weld statistically.

List of Tables

2.1	Summary of important deposition welding processes [Teu02]	5
2.2	Standards for Tubular cored electrodes	10
2.3	Common core elements in flux cored electrodes [Ame91]	12
4.1	Chemical composition	29
4.2	Equipment for the electric circuit	31
4.3	Welding parameters - short circuit	32
4.4	Welding parameters - pulsed mode	32
4.5	Welding parameters - spray mode	33
5.1	Evaluation of the weld seam appearance	41
5.2	Evaluation of the weld seam appearance	41
5.3	Evaluation of the weld seam appearance, pulsed mode with additional shielding gas	52
5.4	Evaluation of the weld seam appearance, self shielded pulsed mode	52
A.1	Parameterlist - short circuit	LXIV
A.2	Parameterlist - spray mode, additional argon shielding gas	LXV
A.3	Parameterlist - pulsed mode, with additional shielding gas (80%-Ar, 20%-CO ₂)	LXVI
A.4	Parameterlist - pulsed mode, without additional shielding gas	LXVII

List of Figures

2.1	Schematic illustration of the tribological system (see [WD11])	2
2.2	Designations of main group 5 of the norm DIN 8580 [DIN03]	4
2.3	Scheme of shielded FCAW [DIN05]	8
2.4	Scheme of self-shielded FCAW [DIN05]	8
2.5	Characteristics of arc length and the power supply	9
2.6	Flux of the current within the arc	11
2.7	Forces acting on the droplet [Dil06]	13
2.8	Transfer modes in an $I - U$ - Diagram [IQ08]	14
2.9	Arc transfermodes according to [IQ08]	14
2.10	Pulsed GMAW current according to Wemann [WL06]	16
2.11	Schematic illustration of the influence of shielding gases of the weld bead formation [Sch10]	17
2.12	Schematic illustration of oscillating torch	19
2.13	Relationship between oscillation frequency and penetration depth and bead width in bead-on-plate welding [KGKI01]	19
2.14	Longitudinal magnetic field	21
2.15	Transversal magnetic field	21
2.16	Axial magnetic field	21
2.17	The influence of the magnetic oscillation on the weld, spray mode . . .	22
2.18	Microstructure near fusion line of 2014 aluminum, 200x [Kou03]	24
2.19	Resulting travel speed according to [KL85]	25
2.20	Influence of the amplitude of the grain size by torch vibration [Kou03, DG75]	25
4.1	Cross section of the wire - SEM analysis	28
4.2	Experimental setup	30
4.3	Schematic illustration of the position of the yoke and welding gun . . .	30
4.4	Schematic illustration of the electrical circuit	30
4.5	Schematic illustration of the position of the sensor of the tesla meter . .	30
4.6	Dimension of the sample	31

4.7	Distance between the centerline of the wire and deflected arc	33
4.8	Schematic illustration of the dimensions of a sample	34
4.9	Schematic illustration of the hardness measuring points	35
5.1	Schematic illustration of the dimensions of a sample	36
5.2	Distribution of the magnetic field density from the distance of the centerline	36
5.3	Material transfer during short circuit for FCAW [Kra]	37
5.4	Comparison of arc deflection due magnetic oscillation	38
5.5	Characteristic drop formation	38
5.6	Acting Lorentz forces deflects the molten tip of the arc	39
5.7	Impact of the magnetic field on the short circuiting arc current character- istic	40
5.8	Influence of the magnetic field on the weld seam appearance	41
5.9	Transversal cracks in the weld seam	42
5.10	Changed process window due to the magnetic oscillation	42
5.11	Influence of the magnetic field on the penetration and width, $I = 210 \text{ A}$, $U = 24.1 \text{ V}$	43
5.12	Influence of the magnetic field on the penetration and width, $I = 260 \text{ A}$, $U = 24.8 \text{ V}$	43
5.13	Cross section of sample D17	45
5.14	Cross section of the control sample D15	45
5.15	SEM analysis of sample D51, $I = 260 \text{ A}$, $U = 24.8 \text{ V}$, $f = 5 \text{ Hz}$, $B = 6 \text{ mT}$	46
5.16	Influence of the magnetic field on the hardness, short circuit	47
5.17	Material transfer during pulsed mode for FCAW [Kra]	48
5.18	Material transfer during pulsed mode for FCAW with magnetic oscillation, $f = 20 \text{ Hz}$, $B = 5 \text{ mT}$ [Kra]	48
5.19	Influence of the magnetic field density and frequency on the arc deflection	49
5.20	Deflection of the arc during pulsed mode	49
5.21	Impact of the magnetic field on the pulsed arc current characteristic . .	50
5.22	Changed Lorentz force acting on the droplet	50
5.23	Weld seam appearance for pulsed mode with additional shielding gas .	51
5.24	Weld seam appearance for pulsed mode, self shielding process	52
5.27	Cross section of sample E27; $f = 25 \text{ Hz}$ and $B = 4 \text{ mT}$	55
5.28	SEM analysis sample E16; $f = 45 \text{ Hz}$ and $B = 6 \text{ mT}$	56
5.29	Influence of LMF on hardness, pulsed mode	57
5.30	Material transfer during spray mode for FCAW [Kra]	58

5.31 Material transfer during spray mode for FCAW, $f = 10\text{ Hz}$ and $B = 10\text{ mT}$, [Kra]	58
5.32 Influence of the magnetic field on the weld seam appearance, spray mode	59
5.33 Cross section, spray mode, $f = 2\text{ Hz}$, $B = 2\text{ mT}$	59



List of abbreviations and formula symbols

Symbol/Abbreviation	Designation	Unit
B	Magnetic flux density	T
C	Capacitance	F
F	Force	N
f	Frequency of the magnetic field	Hz
F_L	Lorentz force	N
I_{base}	Base current	A
I_{peak}	Peak current	A
L	Inductance	H
R	Electrical resistance	Ω
U	Voltage	V
v_{travel}	Travel speed	cm/min
v_{wire}	Wire feeding rate	m/min
f	Frequency of the pulsed transfer mode	Hz
FCAW	Flux cored arc welding	
GMAW	Gas metal arc welding	
LMF	Longitudinal Magnetic Field	
LMO	Longitudinal Magnetic Oscillation	
SAW	Submerged arc welding	
SMAW	Shielded gas metal arc welding	
TMF	Transversale Magnetic Field	
TMO	Transversale Magnetic Oscillation	

Bibliography

- [AC52] AVERY, H. S. ; CHAPIN, H.J.: Hard-Facing Alloys of the Chromium Carbide Type. In: *Welding Journal* 31 (1952), p. 917
- [AK72] AKULOV, A. I. ; KOPAEV, B. V.: Magnetic control of the arc in consumable electrode welding in argon. In: *Automatic Welding* 25 (1972), No. 7, p. 39–42
- [Ame91] AMERICAN WELDING SOCIETY: *Welding Handbook 2: Welding processes*. 8th Edition. Miami : American Welding Society, 1991. – ISBN 0871713543
- [AO83] ASM INTERNATIONAL HANDBOOK COMMITTEE ; OLSON, D.L.: *ASM Handbook Volume 6: Welding, brazing, and soldering*. 9th Edition. ASM International, 1983. – ISBN 9780871703828
- [AO93] ASM INTERNATIONAL HANDBOOK COMMITTEE ; OLSON, D.L.: *ASM Handbook Volume 6: Welding, brazing, and soldering*. 10th Edition. ASM International, 1993. – ISBN 9780871703828
- [Blu00] BLUNT, F. J.: Magnetic arc oscillation for weld surfacing, using mechanised TIG, MIG and PTA processes. Cambridge : Welding Institute, 2000 (Core research from TWI). – ISBN 1855735172
- [BOC07] BOC: *World of Welding Library - 4 Welding Processes*. Product Catalog. Version: 2007. <http://www.bocworldofwelding.com.au/library>
- [DG75] DAVIES, G. J. ; GARLAND, J. G.: Solidification Structures and Properties of Fusion Welds. In: *International Materials Reviews* 20 (1975), No. 1, p. 83–108
- [Dil76] DILTHEY, U.: *Beitrag zur Lichtbogensteuerung durch transversale Zusatzmagnetfelder bei mechanisierten Lichtbogenschweisverfahren*. Aachen, Germany, RWTH Aachen, Ph.D.-Thesis, 1976
- [Dil06] DILTHEY, U.: *Schweißtechnische Fertigungsverfahren 1: Schweiß- und Schneidtechnologien*. 3rd Edition. Berlin, Heidelberg, New York : Springer, 2006. – ISBN 9783540216735
- [DIN03] Norm DIN 8580 2003. *Manufacturing processes*

- [DIN05] Norm DIN EN 14610 2005. *Welding and allied processes – Definitions of metal welding processes*
- [FSTW11] FAHRENWALDT, H.J. ; SCHULER, V. ; TWRDEK, J. ; WITTEL, H.: *Praxiswissen Schweißtechnik: Werkstoffe, Prozesse, Fertigung*. 4th Edition. Wiesbaden : Vieweg+Teubner Verlag, 2011. – ISBN 9783834815231
- [Geb98] *Entwicklung korrosionsbeständiger Auftragschweißschichten mit hoher Verschleißfestigkeit auf Eisenbasis*. Schmalkalden, 1998 (10626 B)
- [Ges] GESELLSCHAFT FÜR TRIBOLOGIE: *Tribologie*. <http://www.gft-ev.de/tribologie.htm>, Last viewed: 21.04.2013
- [HW85] HUGHES, R. ; WALDUCK, R.: Electromagnetic arc path control in robot plasma welding. In: *The International Journal of Advanced Manufacturing Technology* 1 (1985), No. 1, p. 9–25
- [IQ08] IORDACHESCU, Danut ; QUINTINO, Luisa: Steps toward a new classification of metal transfer in gas metal arc welding. In: *Journal of Materials Processing Technology* 202 (2008), No. 1–3, p. 391–397
- [JS00] J. SCHUPP, H. M. W. Fischer F. W. Fischer: *Welding arc control with power electronics* IEE, 2000
- [KGKI01] KODAMA, M. ; GODA, H. ; KAWANO, T. ; IWABUCHI, H.: Compact, lightweight, high-frequency oscillation device using electromagnetic force and corresponding bead formation phenomena. Development of high-frequency oscillating arc (1st report). In: *Welding International* 15 (2001), No. 4, p. 266–274
- [KL85] KOU, S. ; LE, Y.: Improving weld quality by low frequency arc oscillation. In: *Welding Journal* 64 (1985), No. 3, p. 51–55
- [KMSC72] KUZNETSOV, V. D. ; MALINKIN, I. V. ; SYROVATKA, V. V. ; CHERNYSH, V. P.: Behaviour of the arc, and transfer of electrode metal, during welding in a longitudinal magnetic field. In: *Welding Production* 19 (1972), No. 4, p. 4–7
- [KN90] KOBAYASHI, H. ; NAKAHARA, S.: The effects of filler wire and magnetic control in MIG arc welding. In: *Welding International* 4 (1990), No. 10, p. 761–767

- [KN02] KANG, Y. H. ; NA, S. J.: A study on the modeling of magnetic arc deflection and dynamic analysis of arc sensor - A magnetic field applied to a welding arc produced an output signal beneficial for an arc sensor. In: *Welding Journal* 81 (2002), No. 1, p. 8s–13s
- [KN03] KANG, Y. H. ; NA, S. J.: Characteristics of welding and arc signal in narrow groove gas metal arc welding using electromagnetic arc oscillation. In: *Welding Journal* 82 (2003), No. 5, p. 93–99
- [Kou03] KOU, S.: *Welding Metallurgy*. Second Edition. Hoboken, New Jersey : Wiley-Interscience, 2003. – ISBN 0–471–43491–4
- [Kra] KRAUSSER, Stefan: *Untersuchungen zum magnetisch beeinflussten MSG-Fülldrahtschweißen von Hartpanzerungen*, TU Ilmenau, Bachelor Thesis - unpublished
- [Kra00] KRAUSE, W. ET AL. ; KRAUSE, W. (Ed.): *Gerätekonstruktion: in Feinwerktechnik und Elektronik*. 3rd Edition. München, Wien : Hanser, 2000. – ISBN 3446196080
- [MBRM12] MAHAJAN, S. ; BIRADAR, N. S. ; RAMAN, R. ; MISHRA, S.: Effect of Mechanical Arc Oscillation on the Grain Structure of Mild Steel Weld Metal. In: *Transactions of the Indian Institute of Metals* 65 (2012), No. 2, p. 171–177
- [Mer11] MERKLE SCHWEISSANLAGEN-TECHNIK GMBH: *Automation*. product catalog, 06 2011
- [PK81] PEARCE, B. P. ; KERR, H. W.: Grain refinement in magnetically stirred GTA welds of aluminum alloys. In: *Metallurgical Transactions B* 12 (1981), No. 3, p. 479–486
- [Raz95] RAZMYSHLYAEV, A. D.: Controlling the geometrical dimensions of the weld in arc welding and surfacing under the effect of magnetic fields. In: *Welding International* 9 (1995), No. 4, p. 323–325
- [RMS99] RAM, G. D. J. ; MURUGESAN, R. ; SUNDARESAN, S.: Fusion zone grain refinement in aluminum alloy welds through magnetic arc oscillation and its effect on tensile behavior. In: *Journal of Materials Engineering and Performance* 8 (1999), No. 5, p. 513–520
- [SAF11] SAF OERLIKON UK LTD.: *Weldycar NV*. product catalog, 04 2011

- [Sch10] SCHULZE, G.: *Die Metallurgie des Schweißens: Eisenwerkstoffe- Nichteisenmetallische Werkstoffe*. 4th Edition. Berlin, Heidelberg : Springer, 2010. – ISBN 9783642031823
- [She69] SHEINKIN, M. Z.: Use of magnetic oscillations of the arc in submerged-arc welding. In: *Svar Proiz* (1969), No. 6, p. 24–25
- [Sol07] SOLDEXA: *Datasheet of the FCAW wire Exatube 1000-O*. Datasheet, 2007
- [Teu02] TEUPKE, S. E.: *Entwicklung vanadinkarbidhaltiger Schweißzusätze auf Eisenbasis für den Schutz gegen komplexe Beanspruchungen*. Clausthal, Technische Universität, Diss., 2002
- [Tew99] TEWARI, S. P.: Effects of Oscillation on Impact Property of Weldments. In: *ISIJ International* 39 (1999), No. 8, p. 809–812
- [WD11] WEISSBACH, W. ; DAHMS, M.: *Werkstoffkunde: Strukturen, Eigenschaften, Prüfung*. 16th Edition. Wiesbaden : Vieweg+Teubner Verlag, 2011. – ISBN 9783834815873
- [WL06] WEMAN, K. ; LINDEN, G. U.: *MIG Welding Guide*. 1st Edition. Cambridge : Woodhead Publishing Limited, 2006. – ISBN 978-1-85573-947-5
- [WNE89] WATANABE, T. ; NAKAMURA, H. ; EI, K.: Grain refinement by TIG welding with electromagnetic stirring - a study of solidification control of austenitic stainless steel weld metal. In: *Welding International* 3 (1989), No. 4, p. 312–317
- [YGZS12] YIN, Xianqing ; GOU, Jianjun ; ZHANG, Jianxun ; SUN, Jiangtao: Numerical study of arc plasmas and weld pools for GTAW with applied axial magnetic fields. In: *Journal of Physics D: Applied Physics* 45 (2012), No. 28, p. 285203
- [YZG⁺02] YONGBING, L. ; ZHONGQIN, L. ; GUANLONG, C. ; YASHENG, W. ; SHENGYIN, X.: Study on moving GTA weld pool in an externally applied longitudinal magnetic field with experimental and finite element methods. In: *Modelling and Simulation in Materials Science and Engineering* 10 (2002), No. 6, p. 781–798